Annals of Botany **135**: 1475–1496, 2025
https://doi.org/10.1093/aob/mcae228, available online at www.academic.oup.com/aob

ANNALS OF BOTANY
Nonprofit since 1887

ORIGINAL ARTICLE

Global diversification of the common moonwort ferns (*Botrychium lunaria* group, Ophioglossaceae) was mainly driven by Pleistocene climatic shifts

Vinciane Mossion[1,2,*], Erik J. M. Koenen[3], Jason Grant[2], Daniel Croll[2], Donald R. Farrar[4] and Michael Kessler[3]

[1]Department of Ecology and Genetics, Uppsala University, Uppsala, Sweden, [2]Laboratory of Evolutionary Genetics, University of Neuchâtel, Neuchâtel, Switzerland, [3]Department of Systematic and Evolutionary Botany, University of Zurich, Zurich, Switzerland and [4]Department of Ecology, Evolution and Organismal Biology, Iowa State University of Science and Technology, Ames, USA
[*]For correspondence. E-mail vinciane.mossion@ebc.uu.se

Received: 8 September 2024 Returned for revision: 27 November 2024 Editorial decision: 20 December 2024 Accepted: 26 December 2024

• **Background and Aims** The cosmopolitan *Botrychium lunaria* group belongs to the most species-rich genus of the family Ophioglossaceae and was considered to consist of two species until molecular studies in North America and northern Europe led to the recognition of multiple new taxa. Recently, additional genetic lineages were found scattered in Europe, emphasizing our poor understanding of the global diversity of the *B. lunaria* group, although the processes involved in the diversification of the group remain unexplored.
• **Methods** We conducted the first global phylogenetic study of the group, including 533 ingroup accessions sequenced for four plastid loci. We compared results of Bayesian and maximum likelihood-based methods. We used the phylogenetic relationship we recovered to estimate the timing of divergence with BEAST. We explored ecological segregation between species with climatic variables (CHELSA database) and soil pH measurements. The ploidy level and genome size were estimated with flow cytometry.
• **Key Results** We recovered nine well-supported clades, although relationships between clades were inconsistent between Bayesian and maximum likelihood analyses. We treated each clade at the species level, except for one clade including two ploidy levels and one including two recognized diploid species, one of which appeared as a subclade (*Botrychium nordicum*) of the other (*B. lunaria*), resulting in the recognition of 11 species, 4 of which are unnamed. In contrast to previous studies, we found species diversity to be distributed equally across the Northern Hemisphere, with six to eight species per continent. We estimated the stem age of the *B. lunaria* group at 2.5–5.3 Myr, with most species 1.5–2.6 Myr old and subclades 0.2–1.0 Myr old. Diversification thus coincided with Pleistocene climatic fluctuations that strongly affected the areas inhabited by the group, suggesting that diversification was driven by climatically induced cycles of extinction, dispersal and migration. Furthermore, ecological differentiation between species suggests that these complex population dynamics were associated with adaptations to specific environmental conditions. We found limited evidence that speciation is driven by polyploidization and hybridization.
• **Conclusions** The *B. lunaria* group radiation was most probably driven by the Pleistocene climatic shifts. For the first time, we show that ecological drivers might have played a role in the diversification of this group, rather than polyploidization. Furthermore, the *B. lunaria* group has greater species-level diversity than previously assumed, and we suspect that further cryptic species might await discovery, especially in the *B. neolunaria* clade.

Key words: Ophioglossaceae, ferns, speciation, phylogenetics, climate, ploidy, *Botrychium lunaria*, genome size, diversification.

INTRODUCTION

Ferns are an ancient group of vascular plants, with fossil records dating back to the middle Devonian (387.7–382.7 Myr) (Berry and Hilton, 2006; Taylor *et al.*, 2009) and divergence from the seed plants estimated at ~360–430 Mya (Wikström and Kenrick, 2001; Des Marais *et al.*, 2003; Pryer *et al.*, 2004; Magallón *et al.*, 2013; Zhong *et al.*, 2014; Rothfels *et al.*, 2015; Testo and Sundue, 2016; Lehtonen *et al.*, 2017; Qi *et al.*, 2018). Devonian fern lineages, such as Cladoxylopsida or

Rhacophytales (Taylor *et al.*, 2009), have long gone extinct, and most of the ~11 000 extant fern species arose from a Cenozoic radiation (Schneider *et al.*, 2004; Schuettpelz and Pryer, 2009; Testo and Sundue, 2016). The recent nature of extant fern species and their overall slow (Smith, 1972) but heterogeneous (Rothfels *et al.*, 2012; Testo and Sundue, 2016) rates of diversification imply that many groups comprise species complexes characterized by morphologically poorly defined species (Paris *et al.*, 1989: p. 198; Williams *et al.*, 2016; Vasques *et al.*, 2019) often in combination with polyploid networks (Lovis, 1958; Chang *et al.*, 2013; Rothfels *et al.*, 2014; Williams *et al.*, 2016; Hanušová *et al.*, 2019). In such a context, interpreting species diversity and understanding the speciation processes involved in diversification are challenging and intriguing.

The Ophioglossaceae are a good example of an ancient fern family, with a divergence time estimated at 262–322 Mya (Testo and Sundue, 2016; Kumar *et al.*, 2017; Lehtonen *et al.*, 2017), composed of recently diverged species (Rothfels *et al.*, 2015; Lehtonen *et al.*, 2017; Dauphin *et al.*, 2018), many of which are genetically distinct but morphologically hardly distinguishable (Hauk, 1995; Dauphin *et al.*, 2017; Zhang *et al.*, 2020). Ophioglossaceae are characterized by subterranean gametophytes that are colonized by mycorrhizal fungi (Winther and Friedman, 2007) and by an unusual sporophyte leaf morphology: the yearly leaf is composed of a sterile photosynthetic blade, the trophophore, and of a fertile portion, the sporophore (Fig. 1A). This simple morphology provides only a limited number of distinctive features, making morphological differentiation of species challenging (Stensvold, 2007; Farrar, 2011; Williams and Waller, 2015, 2016). Accordingly, the number of species recognized historically in the family has been low. Clausen (1938) recognized only six species in *Botrychium s.s.* (subgenus *Eubotrychium*). Later, Wagner (Wagner and Wagner, 1981, 1982, 1983*a*, 1986, 1990*a*, *b*, 1994; Wagner and Grant, 2002) and other taxonomists (Farrar and Johnson-Groh, 1991; Stensvold *et al.*, 2002; Mickel and Smith, 2004; Gilman *et al.*, 2015; Stensvold and Farrar, 2017; Popovich *et al.*, 2020), using cytology, allozyme data and detailed morphological analyses, gradually increased the number of taxa to 36 currently (PPG I, 2016; Dauphin *et al.*, 2017), of which 30 have been described in the last four decades. The newly defined species exhibit subtle morphological differences, often along with geographical and ecological distinctness. More recently, phylogenetic analysis based on plastid markers (*rbcL*, *trnL-F*, *rpl16* intron, *psbA-trnH*^{GUG} and *matK* region) (Hauk, 1995; Hauk *et al.*, 2003, 2012; Dauphin *et al.*, 2014, 2017) uncovered further lineage diversity within *Botrychium*, especially among the European populations treated as *Botrychium lunaria* (L.) Sw. (Dauphin *et al.*, 2014, 2017; Maccagni *et al.*, 2017). These findings suggested that deeper investigations on *B. lunaria* populations might shed further light on the diversity within the group.

The *Botrychium lunaria* group is one of three monophyletic clades within *Botrychium*, called the Lunaria clade by (Dauphin *et al.*, 2014). It includes what was long considered to be a single, morphologically variable species that occurs across the boreal and alpine regions of North America, Europe and Asia, with outposts in New Zealand and Australia (Milde, 1869: p. 7; Clausen, 1938; Kato, 1987). As early as 1903, Underwood suggested that at least two distinct taxa occurred in North America, prompting his description of *Botrychium onondagense*. However, subsequent studies treated *B. onondagense* as a variety or form of a *B. lunaria* (Clute, 1905; Clarke and House, 1921; Clausen, 1938; Butters and Abbe, 1953). Later, based on extensive morphological surveys, Wagner and Wagner, (1981) described *Botrychium crenulatum*, a North American species that has been widely accepted (Dauphin *et al.*, 2017; Farrar *et al.*, 2017; Stensvold and Farrar, 2017). When allozyme markers were used more extensively and the investigation area was extended to northern Europe, five additional taxa were recognized (*Botrychium tunux*, *B. nordicum*, *B. neolunaria*, *B. yaaxudakeit* and *B. lunaria* var. *melzeri*) (Stensvold *et al.*, 2002; Stensvold and Farrar, 2017). The recognition of *B. neolunaria* as the common *B.* '*lunaria*' in North America re-evaluated Underwood's *B.* '*onondagense*' as the North American representative of European *B.* '*lunaria*'. Until a few years ago, most taxa in the *B. lunaria* group were from North America. More recently, however, it has been found that the genetic diversity among *B.* '*lunaria*' populations in western and central Europe might exceed the diversity found in North America (Dauphin *et al.*, 2014, 2017; Maccagni *et al.*, 2017). Some European lineages could be assigned to species previously described from North America, such as *B. tunux* (Stensvold *et al.*, 2002). Yet, there remain several poorly understood lineages within *Botrychium* possibly representing additional species (Dauphin *et al.*, 2017). These hitherto undescribed lineages are widespread throughout Europe, highlighting the uncertainty of taxonomic assignments of European *B.* '*lunaria*' and the limited understanding of the global diversity of the *B. lunaria* group.

Significant advances have been made to understand speciation processes within *Botrychium*. Polyploidization appears to be a major factor in some clades of *Botrychium*, and complex polyploid networks have been uncovered (Wagner and Lord, 1956; Wagner, 1993; Williams and Waller, 2012; Dauphin *et al.*, 2016), but the relevance of polyploidization in the *B. lunaria* group remains unclear. Among the 36 accepted *Botrychium* species, nearly half are allopolyploids. Of the new taxa in the *B. lunaria* group, *B. yaaxudakeit* is noteworthy as the only allopolyploid species discovered in the group. Using allozyme analysis, Stensvold *et al.* (2002) found that *B. yaaxudakeit* carries a combination of alleles matching *B.* '*lunaria*' and *B. neolunaria* and shows morphological intermediacy. Scattered sampling in North America and central Europe (Veselý *et al.*, 2012; Williams and Waller, 2012; Dauphin *et al.*, 2016) found no further evidence of polyploids in the *B. lunaria* group, suggesting that the speciation processes involved in the diversification of this group might differ from other *Botrychium* clades. However, diploid hybrids between *B. neolunaria* and *B.* '*lunaria*' have been detected by allozyme markers in North America, in western and northern Europe, and on the east coastline of Asia and Oceania (Stensvold *et al.*, 2002; Stensvold and Farrar, 2017). These hybrids, commonly called introgressed hybrids, originate from the germination of spores produced by F1 hybrids. The term reflects the unequal contributions by the two diploid parents during the meiosis. Introgressed hybrids are diploid and fertile plants, which are supposedly as reproductively isolated from their parents as allotetraploids are. The success of the hybrids suggests that introgression might favour rapid speciation by promoting adaptive divergence (Abbott *et al.*, 2013). Phylogenetic analysis of plastid data showed that although the maternal donor of these hybrids was *B. neolunaria*,

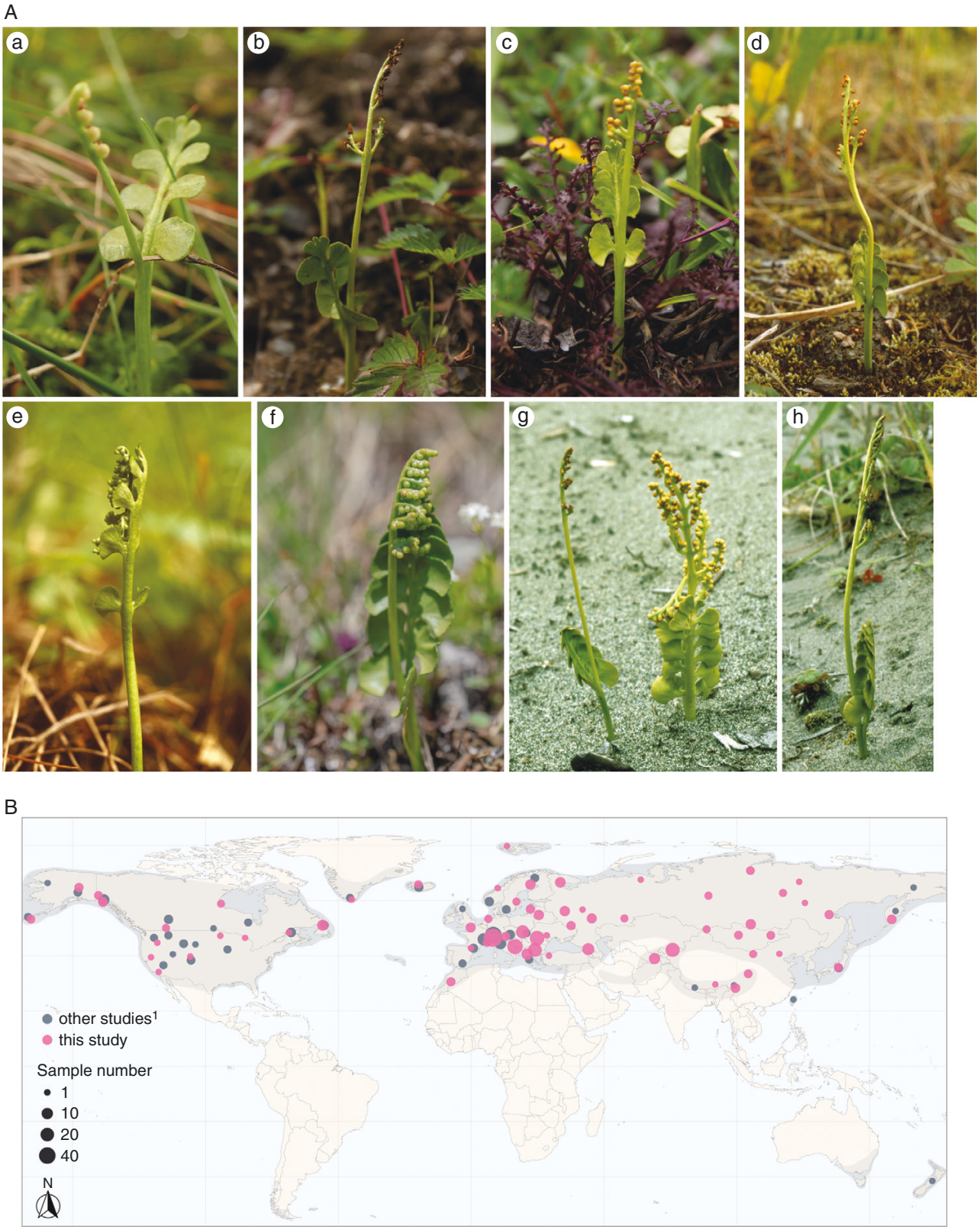

FIG. 1. Morphological diversity of the *Botrychium lunaria* group and geographical distribution of the analysed individuals. (Aa) *Botrychium onondagense* VM-lun26-5-RO (photograph by Q. Dubois, Romania). (Ab) Putative novel species (clade 3) VM-lun55-1-CN (photograph by V. Mossion, China). (Ac) Putative novel species (clade 7) VM-lun54-CN (photograph by V. Mossion, China). (Ad) *Botrychium neolunaria* (photograph by D. Farrar, USA). (Ae) *Botrychium crenulatum* (photograph by D. Farrar, USA). (Af) *Botrychium lunaria*, VM-lun89-CH (photograph by V. Mossion, Switzerland). (Ag) *Botrychium neolunaria s.s.* on the left, *Botrychium tunux* on the right (photograph by D. Farrar, USA). (Ah) *Botrychium yaaxudakeit* (photograph by D. Farrar, USA). (B) Sampling map, differentiating between sequences from previous studies (grey) and this study (pink). The distribution range of the *B. lunaria* group (Stensvold, 2007) is shown by the grey layer. Individuals <500 km apart were clustered and are indicated by a unique circle. The circle sizes are proportional to individual number. [1]Dauphin *et al.* (2014, 2017); Maccagni *et al.* (2017).

hybrids formed a distinct subclade (Dauphin *et al.*, 2017), supporting this idea. Hence, both polyploidization and hybridization events have contributed to the diversification within the *B. lunaria* group, but their specific contributions remain poorly understood.

Diversification within the *B. lunaria* group might have been driven by successive isolation, migration and dispersal events imposed by the Quaternary glacial–interglacial cycles (Stensvold, 2008). The *B. lunaria* group occurs mainly in circumboreal–temperate regions strongly affected by Quaternary glacial cycles (Stensvold, 2008; Ehlers *et al.*, 2011). As in many other boreal and alpine plant groups, this might have led to complex population dynamics (Schönswetter *et al.*, 2005), possibly associated with adaptations to different climatic or soil conditions (Alvarez *et al.*, 2009; Allen *et al.*, 2012; de Lafontaine *et al.*, 2018). For some species of the genus *Botrychium*, local ecological, climatic and edaphic specialization has been reported. For example, populations of *B. campestre* from northeastern Iowa (USA) have slope preferences within habitats (Nekola and Schlicht, 1996), whereas populations of *B. matricariifolium* from Vosges (France) occur on sandy and acid soils, in areas with high annual mean precipitation and cool summers (Muller, 1986). The closely related species *Botrychium simplex* and *Botrychium tenebrosum* that occur in North America, Sweden and Switzerland, also tend to have different preferences for wetter or dryer habitats, respectively (Ståhl *et al.*, 2016; A. Maccagni, pers. comm.). However, these species belong to other clades of *Botrychium*, and little is known on the climatic and edaphic niches of species from the *B. lunaria* group. Ecological niche segregation among two genetic lineages of *B.* '*lunaria*' has been suggested based on habitat preferences in the Alps (Maccagni *et al.*, 2017). In North America, *B. tunux* and *B. yaaxudakeit* favour well-drained soils, whereas *B. neolunaria* grows on poorly to moderately drained substrates (Stensvold *et al.*, 2002; Stensvold and Farrar, 2017). In the absence of further characterization of the ecological niches of the lineages within the *B. lunaria* group, it is currently impossible to address to what degree climatic and edaphic adaptation contributed to the diversification of the group.

In this study, we have analysed the worldwide diversity and diversification time of the *B. lunaria* group and associated the occurrence of individual lineages with climatic and edaphic factors. We performed a plastid-based phylogenetic reconstruction, including a large set of newly collected samples from eastern Europe and Asia. We also investigated genome size variation to identify potential polyploidization events throughout the diversification of the *B. lunaria* group. Specifically, we asked the following questions:

(1) How many species-level lineages can be recognized in the *B. lunaria* group?
(2) What is the species diversity of the group in eastern Europe and Asia?
(3) What is the role of polyploidization in the diversification of the group?
(4) Can the timing of species divergences be related to Pleistocene climatic fluctuations?
(5) Is there ecological differentiation between species that might be linked to the diversification of the group?

MATERIALS AND METHODS

Sample collection

We collected 172 fresh sporophytes at 63 locations within Eurasian Mountain ranges, including 41 sites in central and eastern Europe (Alps, Carpathians, Dinaric Alps, Rhodopes, Central Balkans and Caucasus) and 14 in central and eastern Asia (Pamir-Alay, Tien-San, Eastern Himalayas, Qinling and Yann) (Fig. 1B). At each location, we sampled 3–15 plants ≥20 cm apart, collected soil samples around the roots of one or two individuals, measured the soil pH using a Hellige pH meter and recorded the geographical coordinates at the centre of sampling sites using a Garmin eTrex 30X GPS. From each plant, a few pinnae were silica dried on site and the remaining plant kept as a herbarium voucher. Vouchers were deposited in the herbaria of the University of Zurich (Z/ZT) and University of Neuchâtel (NEU), Switzerland, and in herbaria in the countries of origin (Supplementary Data Table S1). In addition, we also incorporated 203 samples from China, Russia, Europe, North Africa and North America provided by collaborators (see Acknowledgments) and herbaria (PE, MW, AIX, ISC and MARK) (Supplementary Data Table S1), which included type material of five recognized taxa (*B. tunux*, *B. neolunaria*, *B. crenulatum*, *B. yaaxudakeit* and *B. lunaria* var. *melzeri*). The sampling was designed to cover the whole distribution range of the *B. lunaria* group as described by Stensvold (2008) (Fig. 1B).

DNA extraction, amplification and sequencing

We extracted total genomic DNA from silica-dried and herbarium material using the DNeasy plant mini kit (Qiagen, Hilden, Germany). We modified the manufacturer's protocol as follows: the mixture was incubated in buffer AP1 and RNase A for 20 min, a centrifugation step of 1 min at 6000 *g* was added before the centrifugation of the 17th step, and DNA was eluted in ultra-pure water. Total genomic DNA was quantified and quality checked by spectrophotometry (NanoDrop 2000). The four plastid loci targeted (*trnH*^{GUG}-*psbA* intergenic spacer, *trnL*^{UAA}-*trnF*^{GAA} intergenic spacer, *matK* region and *rpl16* intron) were amplified by PCR following protocols and thermocycling conditions published by Dauphin *et al.* (2014, 2017) and Small *et al.* (2005). Besides, we optimized thermocycling conditions for touchdown protocol and the use of a high-fidelity DNA polymerase to amplify degraded DNA extracted from herbarium material (Supplementary Data Table S2). Briefly, the PCRs were performed in a volume of 50 µL containing 10 ng of DNA template, 0.2 µM of each primer (Microsynth, Balgach, Switzerland), 0.2 mM of DNTPs mix (Promega, Madison, WI, USA), 1 unit of GoTaq DNA polymerase (Promega), 1× GoTaq buffer (Promega) and an additional 1 mM of $MgCl_2$ (Promega) for *trnL*^{UAA}-*trnF*^{GAA}. Herbarium material DNAs were amplified using Q5 high-fidelity DNA polymerase with the following PCR product concentrations: 0.3 µM of each primer (Microsynth), 0.2 mM of DNTPs mix (Promega), 0.5 unit of Q5 (New England Biolabs Inc., Ipswich, UK), 1× Q5 buffer (New England Biolabs Inc.) and an additional 1 mM of Q5 enhancer (New England Biolabs

Inc.) for *trnL*^{UAA}-*trnF*^{GAA}. Each PCR product was quality checked by electrophoresis on agarose gel (1.5 %) stained with GelRed® (Biotium, Fremont, CA, USA) and visualized under UV light on a transilluminator (UVI Tec Gel Documentation System). Template purifications and sequencing were outsourced to Macrogen Europe (Amsterdam, The Netherlands). Succinctly, sequencing reactions were performed in the Master Cycler pro 384 (Eppendorf) using the ABI BigDye® Terminator v.3.1 Cycle Sequencing Kit (Applied Biosystems), following the protocols supplied by the manufacturer. Single-pass sequencing was performed on each template using the combination of same primers as for PCR. The fluorescence-labelled fragments were purified from the unincorporated terminators with the BigDye XTerminator® Purification Kit (Applied Biosystems). The samples were injected to electrophoresis in an ABI 3730xl DNA Analyzer (Applied Biosystems). The four regions were paired-end sequenced. The remaining silica material and DNA extractions were deposited at the Botanical Institute of Zurich, Switzerland.

Sequence cleaning and alignment

Sequences were trimmed and ambiguous bases annotated using the default settings of Geneious v.8.1.9 (https://www.geneious.com) *Trim ends* and *Find heterozygotes* plug-ins. Consensus sequences were obtained from paired-end contigs, and uncertain positions were cleaned manually according to the base quality of the chromatograms. In the case of ambiguous bases presenting equal chromatogram quality on both sequences, ambiguity was kept and the base coded according to the International Union of Biochemistry (IUB) code (Cornish-Bowden, 1985). Consensus sequences were aligned per locus using MAFFT v.7.017 (Katoh and Standley, 2013) under the G-INS-i strategy and default parameters. Alignments were inspected visually and curated manually using Geneious. For instance, gaps in low-quality 3′ and 5′ end regions were annotated as missing data. A minority of individuals presented partial sequencing data (6 %; Table 1; Supplementary Data Table S1). Additional published sequences of *Botrychium* (e.g. outgroups, specimens of the synonymized *B. onondagense* and supplementary type material) and of the Botrychioideae subfamily were incorporated into our dataset (Dauphin *et al.*, 2014, 2017; Maccagni *et al.*, 2017; Zhang *et al.*, 2020; Supplementary Data Tables S1 and S3). One-third of these supplementary accessions had information at the *trnH*^{GUG}-*psbA* and *trnL*^{UAA}-*trnF*^{GAA} loci only. The uniparentally inheritance (Gastony and Yatskievych, 1992; Vogel *et al.*, 1998; Guillon and Raquin, 2000; Kuo *et al.*, 2018) and the absence of recombination (Ravi *et al.*, 2008) in fern chloroplasts allowed us to analyse the four targeted loci as a concatenated single locus. Alignments per locus were concatenated using the R v.4.0.3 (R Core Team., 2021) seqinr v.4.2-4 (Charif and Lobry, 2007) package and the *concat* function (Khang, 2016). The ingroup was represented by 533 individuals with type material of each named taxon within the *B. lunaria* group, except for *B. lunaria* and *B. onondagense*. The outgroup contained nine diploid species of the two other *Botrychium* clades (Lanceolatum and Simplex–Campestre) (Supplementary Data Table S1).

Phylogenetic reconstruction

We assessed the phylogenetic relationships within the *B. lunaria* group based on two datasets (i.e. multiple alignment): one containing all the 542 accessions (full dataset, A2; Supplementary Data File S1) and one containing a subset of 274 individuals that excluded 100 samples with partial sequencing data and 168 accessions carrying low phylogenetic signal (rogue individuals) (reduced dataset, A1; Supplementary Data File S2). Rogues were identified using R Rogue package v.2.1.6 (Smith, 2022) with the relative bipartition information content and Pattengale's criterion implemented via RogueNaRok (Aberer *et al.*, 2013). Rogues were identified with 1000 bootstrap trees obtained by performing tree inference on the alignment without partial sequencing (A0) data under the TIM1+I+G4 model and a single partition using RAxML-NG v.1.1.0 (Kozlov and Stamatakis, 2019) (Table 1). For each dataset, the best substitution model was estimated according to the Akaike information criterion (AIC) using ModelTest-NG v.0.1.7 (Darriba *et al.*, 2019), and the best scheme was tested using PartitionFinder 2 (Frandsen *et al.*, 2015), with *branch lengths* set as *unlinked* and the *substitution models* set as *all*. All phylogenetic analyses described hereafter were performed with a single partition following the PartitionFinder 2 best scheme. Unrooted species trees were built with maximum likelihood (ML) using RAxML-NG and Bayesian inference (BI) using Bayesphylogenies 2 (Pagel *et al.*, 2004).

The reduced dataset (A1) was analysed both with and without indels. Indels were scored using the *2 matrix* script (Salinas and Little, 2014), which implemented the simple indel coding algorithm described by Simmons and Ochoterena (2000). In total, 37 informative indels were scored (Supplementary Data File S2). We ran ML inferences under a TIM1+I+G4 substitution model and BIN model for the indels with a fixed random seed of 124. The tree search was performed on 25 random and 25 parsimony-based starting trees, and branch support was estimated over 5000 bootstrap replicates. Bootstrap convergence was tested *post hoc* using the –bsconverge command with a cut-off of 0.03. Bootstrap values were depicted on the best tree using the *Transfer Bootstrap Expectation* metric (Lemoine *et al.*, 2018). BIs were conducted under the GTR+I+G4 substitution model and M1P models for indels using the reversible jump method. We set two runs of 50 million Markov chain Monte Carlo generations, each including one cold and two heated chains, with a seed number of 946 432 and with the tree being sampled every 5000 generations. Parameter files were inspected with Tracer v.1.7 (Rambaut *et al.*, 2018), and a burn-in of 10 % was applied to the analyses. Majority-rule consensus trees of 50% were built based on posterior probabilities (PP) using SumTrees v.4.4.0 and DendroPy library v.4.4.0 (Sukumaran and Holder, 2010).

The full dataset (A2) was analysed with a constraint backbone to minimize the effect of incomplete data and rogue individuals on tree inference. We used the best ML tree of the A1 with and without indels as the constraint backbone. These phylogenetic inferences were performed by ML only under a TPM1uf+I+G4 substitution model with a fixed random seed of 124. The tree search was performed on 25 random and 25 parsimony-based starting trees, and branch support was estimated over 1000 bootstrap replicates, and bootstrapping analysis convergence

TABLE 1. *Characteristics of the multiple alignments, including the outgroup.*

Alignments	Individuals	Alignment sites (bp)	Parsimony-informative sites[1]	Unique sequences[2]	Unique patterns[3]	Gaps (%)[4]	Variable sites (%)[5]	Indels[6]	Indels gaps (%)[7]	Substitution model [8]	Partition[9]	Tree constraint	Bootstrapping analysis convergence
trnH^{GUG}-*psbA*	534	582	139 (114)	–	–	–	–	–	–	–	–	–	–
trnL^{UAA}-*trnF*^{GAA}	520	414	100 (81)	–	–	–	–	–	–	–	–	–	–
matk	490	652	116 (99)	–	–	–	–	–	–	–	–	–	–
rpl16	461	726	157 (142)	–	–	–	–	–	–	–	–	–	–
A0 (no partial sequencing)	442	2374		248	345	3.42	9.27	–	–	ML: TIM1+I+G4	1	–	650
A1 (no partial sequencing, rogue excluded)	274	2374		171	299	3.23	8.70	37	15.05	ML: TIM1+I+G4, BIN BI: GTR+I+G4, M1P	1	–	(indels): 3000 (no indels): 1900
A2 (full)	542	2374	–	313	446	11.52	9.69	–	–	ML: TPM1uf+I+G4	1	A1-indels backbone A1 backbone	350 400
Botrychioideae	20	1588		20	368	2.58	35.9	–	–	Part 1: GTR+I Part 2: GTR+I+G	Part 1: *trnH*^{GUG}-*psbA*, *trnL*^{UAA}-*trnF*^{GAA} Part 2: *matK*	–	–

[1]Number of parsimony-informative sites given by the pis function of R phyloch package. Coded ambiguities are treated as missing data, and calculation is not available for alignments with missing data. The value in parentheses corresponds to the number of parsimony-informative sites while the outgroup was excluded.

[2, 3, 4, 5, 7, 10]These values were reported on Raxml-ng outputs. [6]Number of indels scored by the simple indel coding algorithm.

[8, 9]Optimal substitution models and best scheme selected by ModelTest-NG and PartitionFinder 2 for the ML and the BI analysis. The indels models used (BIN and M1P) were the simplest model available for i.

was tested with the same set-up as for A1. Trees were depicted using R ggtree v.2.4.0 (Yu *et al.*, 2017, 2018), ape v.5.4-1 (Paradis and Schliep, 2019), treeio v.1.14.0 (Wang *et al.*, 2020), ggplot2 v.3.3.3 (Wickham, 2016), tidyverse v.1.3.0 (Wickham *et al.*, 2019), viridis v.0.5.1(Garnier *et al.*, 2024), scales v.1.1.1 (Wickham *et al.*, 2023), ggtreeExtra v.0.4.5 (Xu and Yu, 2021), ggstar v.1.0.1 (Xu *et al.*, 2022), RColorBrewer v.1.1-2 (Neuwirth, 2022) and ggnewscale v.0.4.5 (Campitelli, 2024) packages and Figtree v.1.4.4 (Rambaut, 2009).

Assessment of ploidy level

We assessed the ploidy level of 57 individuals covering the whole phylogeny using flow cytometry following the one-step methodology of Dolezel and Bartos (2005). Briefly, ~0.125 cm^2 of fresh or silica-dried internal standard leaf (*Pisum sativum* 'Ctirad'; 2C = 9.09 pg; Doležel *et al.*, 1998) and 0.125–0.250 cm^2 of silica-dried fern tissue were co-chopped using a fresh razor blade in a Petri dish containing 1 mL of ice-cold Otto I buffer (0.1 M citric acid and 0.5% Tween 20). The resulting suspension was incubated for 15 min at room temperature (20 °C) with occasional shaking and filtered through a 42 µm nylon mesh. The filtrate was stained with 1 mL of Otto II buffer (0.4 M $Na_2HPO_4.12\ H_2O$; fluorochrome 4′,6-diamidino-2-phenylindole: 4 µg mL^{-1}) for 1–2 min at room temperature, after which the relative fluorescence was recorded on a CytoFLEX S (Beckman Coulter, Indianapolis, IN, USA). The excitation beam was provided by a laser tuned to a wavelength of 351 nm. Fluorescence emission was detected by a filter permitting passage of light of wavelength of 450 nm. The 2C-values were calculated by comparing the mean *Botrychium* peak with the mean standard peak. Ploidy levels were also derived from spore sizes (Popovich *et al.*, 2020) for 14 individuals with genetic proximity to the tetraploid *B. yaaxudakeit* and its maternal donor *B. neolunaria* for which silica-dried material was not available. Spore sizes of three *B. neolunaria* and five *B. yaaxudakeit* specimens identified by allozymes (Stensvold, 2008; D. Farrar, unpubl. data) were used as reference. Dried spores were placed in a 1.5 mL Eppendorf tube and suspended in 300 mL of Euparal (Roth, Karlsruhe, Germany) mounting medium. Nine drops of spore solution were distributed equally on a coverslip, on the top of which a slide was gently placed. The slides were dried, coverslip face down, for ≥2 weeks before spore measurement. Spores were photographed using an inverted microscope (Leica DMI3000B). The longest length of the spore was measured on a minimum of ten spores per individual using LAS v.4.13 Leica software and ImageJ v.1.52a (Schneider *et al.*, 2012). The mean and standard deviation of spore lengths were calculated in R.

Species delimitation

Here, we follow the taxon concept of De Queiroz (2007), which defines taxa as independently evolving metapopulation lineages. The monophyletic clades corresponding to previously accepted species were treated as such, and those representing unnamed entities were considered as putative species (Solís-Lemus *et al.*, 2015; Sukumaran and Knowles, 2017). Well-supported monophyletic subclades nested within putative species were highlighted and discussed. Species status of clades was evaluated further by coherent geographical distribution and/or distinct ecological features, in combination with previously published information on reproductive isolation between taxa, when available (Wagner and Wagner, 1983*b*).

Divergence time

We estimated divergence times within the *B. lunaria* group in a two-step time calibration. First, we estimated the divergence time of the *Botrychium* crown, and second, we inferred the divergence times of the *B. lunaria* group with the *Botrychium* crown age as a secondary derived calibration. In the first step, we analysed the concatenated alignment of the subfamily Botrychioideae (Supplementary Data File S3; Table S3) under strict and uncorrelated lognormal relaxed clock models using BEAST v.1.10.4 (Drummond *et al.*, 2012). The alignment was partitioned according PartitionFinder 2 output (Table 1), and the site models were unlinked. A birth–death *tree prior* was applied, with a given starting tree as *tree model*. The starting tree was built using RAxML-NG and transformed into an ultrametric tree using the penalized likelihood method (Sanderson, 2002) implemented in the chronopl function of the R ape v.5.4-1 package. The *clock rate* or the *ucldMean* priors were set with an exponential distribution and default parameters. We used two macrofossils to constrain the stem ages of the *Botrypus virginianus* and *Sceptridium* (Rothwell and Stockey, 1989; Bozukov *et al.*, 2010). Morphological analysis related the youngest fossil to *Sceptridium underwoodianum* (Bozukov *et al.*, 2010), whereas the oldest fossil was described as an extinct species, *Botrychium wightonii* Rothwell & Stockey, related to *Botrypus virginianus* (Rothwell and Stockey, 1989). We applied to the *tmrca priors* a uniform distribution, with the minimum age of fossils as lower boundaries (56.8 and 20.44 Myr, respectively) and the Ophioglossaceae family age estimated by Lehtonen *et al.* (2017) as upper boundaries (148.9 Myr). We set a normal distribution for the *treemodel-rootheight* prior with a mean age of 148.9 Myr (Lehtonen *et al.*, 2017) and an s.d. of 1.0 Myr, and we truncated it with an upper boundary in the middle Jurassic (175.6 Myr). We constrained the calibrated clades as monophyletic and set *Helminthostachys zeylanica* as an outgroup of the subfamily Botrychioideae to facilitate the convergence of the analysis. We ran one analysis per clock model of 20 and 50 million Markov chain Monte Carlo generations for the strict and the relaxed clock, respectively, with parameters sampled every 1000 generations. Besides, those two analyses were performed without sequence data and without fossil calibrations to control the influence of the priors on the time divergence estimates.

Second, we analysed the A1 alignment containing only unique sequences created by RAxML-NG (Supplementary Data File S4) under strict and uncorrelated lognormal relaxed clock models using BEAST. A Yule *tree prior* was applied, with a given starting tree as *tree model*. The starting tree was built with the same method as the Botrychioideae starting tree. The *clock rate* or the *ucldMean* priors were set with an exponential distribution and default parameters, and the *site model* with GTR+G.

We set the distribution parameters using the time divergence estimates of the genus *Botrychium* given by the analysis of the subfamily Botrychioideae. The *treemodel-rootheight* priors were defined by a normal and a gamma distribution for the strict and the relaxed clock, respectively. The normal distribution had a mean of 14.1 Myr, an s.d. of 1.6 Myr, and we truncated it with an upper boundary of 20.7 Myr (upper range boundary of *Botrychium* mean). The gamma distribution had a *shape* of 19.5 Myr (mean age), a *scale* of 0.7, and we truncated it with an upper boundary of 73.1 Myr. We constrained the calibrated clade as monophyletic to facilitate the convergence of the analysis. We ran one analysis per clock model of 50 million Markov chain Monte Carlo generations, with parameters sampled every 1000 generations.

The convergence of all analyses was inspected in Tracer v.1.7.1. The effective sample size of every parameter was >200, and we defined a burn-in of 10 %. We summarized our post burn-in trees using TreeAnnotator v.1.10.4 (Drummond *et al.*, 2012) to generate a maximum clade credibility tree. Besides, we sampled priors for 100 million generations and compared the time divergence estimates with those obtained with the run including the data to ensure the estimates were not driven by priors. Trees were depicted using R ape, phytools v.0.7-70 (Revell, 2012), treeio, ggtree, ggplot2, deeptime v.0.0.5.3 (Gearty, 2024) and strap v.1.4 (Bell and Graeme, 2014) packages. The densitrees were drawn using subsamples of 90 posterior trees obtained with Logcombiner v.1.10.4 (Drummond *et al.*, 2012).

Distribution ranges and climatic analysis

We used 509 genotyped individuals with geographical coordinates to define species distribution ranges. The species distribution ranges were visualized using R ggplot2, sf v.0.9-7 (Pebesma, 2018), ggspatial v.1.1.5 (Dunnington, 2025), rnaturalearth v.0.1.0 (South, 2017) and RColorBrewer packages.

We extracted the 19 bioclimatic variables from CHELSA (Karger *et al.*, 2017, 2018) for the collecting localities of 239 individuals, a subset of the reduced dataset samples, from which we excluded individuals with inaccurate geographical coordinates and samples identified by allozymes as introgressed hybrids (Stensvold, 2008; D. Farrar, unpubl. data; Supplementary Data Table S1). The subset of individuals covered all accepted and putative species and the subclades we considered, except for subclade 2, which had an insufficient number of geo-referenced individuals to be considered in the analysis. The variable scales varied widely, and because variables such as the minimum temperature of the coldest month (BIO 6) had negatives values, log transformation could not be applied uniformly. Thus, we normalized the data using the *z*-score standardization. The overall differences between taxa were visualized for each bioclimatic variable with boxplot representations (Supplementary Data Fig. S1). The variables showing differences between taxa and subclades were identified using ANOVA (Supplementary Data Folder 1, Files S5–S7). We retained 18 of 19 variables for the analysis at the species level (BIO 9 was excluded) and 3–14 variables for the analysis at the subclade level (Supplementary Data Folder 1, Files S8–S16). To visualize the climatic niches of both species and subclade, we performed principal component analyses (PCAs) to account for covariance between climatic variables (Supplementary Data Files S8–S16, Supplementary Data Folder 1). The data normalization was done using R *scale* function, and analyses were conducted using the R rstatix v.0.6.0 (Kassambara, 2023b) and FactoMineR v.2.4 (Lê *et al.*, 2008) packages. The data and results were visualized using the R ggplot2 tidyverse and factoextra v.1.0.7 (Kassambara and Mundt, 2020), cowplot v.1.1.1 (Wilke, 2024) and ggpubr v.0.4.0 (Kassambara, 2023a) packages.

Soil pH measurements obtained through field expeditions (see sampling collection section) were refined by measurements realized in the soil biology laboratory of the University of Neuchâtel. Briefly, soil samples were dried at 40 °C. Then, one volume of dried soil was mixed with 2.5 volumes of water and stirred three times for 5 s with 20 min between each. The pH was measured 20 min after the last agitation using a 914 pH/Conductometer (Metrohm SA, Zofingen, Switzerland). In total, we measured soil pH for 50 populations represented by 54 samples covering seven of the nine clades (Supplementary Data Table S1). The association patterns of soil pH and species were visualized with boxplots using R ggplot2 and tidyverse packages.

RESULTS

Locus diversity and plastid-based phylogenetic analysis

The concatenated plastid DNA regions consisted of 2374 aligned nucleotides, of which ~12 % and 18 % were parsimony-informative sites for A1 and A2, respectively (Table 1). A reasonable proportion of individuals (>80 %) were analysed at all four target loci (Supplementary Data Table S1). The loci were not equally informative (Table 1). The *trnH*^{GUG}-*psbA* intergenic spacer and the *rpl16* intron were the most variable (114 and 142 parsimony-informative sites, respectively), whereas the *trnL*^{UAA}-*trnF*^{GAA} intergenic spacer was the least informative (81 sites). However, the *rpl16* intron presented the lowest sampling completeness owing to repeated PCR amplification failure and limited availability of published data (Table 1; Supplementary Data Table S1).

The phylogenetic analysis recovered nine well-supported monophyletic clades inside the *B. lunaria* group (Fig. 2; for tip labels and support values of all branches, see Supplementary Data Figs S2 and S3; Files S17 and S18), consistently arranged into three to four main groups of clades (Figs 2B, C and 3; Supplementary Data Fig. S2). The first group included three clades (clades 3–5), one included a unique clade (clade 9), another included two clades (clades 2 and 7), which also contained clade 9 in the tree inference based on the full dataset, and the last included three large clades (clades 1, 6 and 8). The trees resulting from the ML and BI analysis based on the reduced dataset (A1) retrieved the same main groups of clades (Fig. 3; Supplementary Data Files S17 and S18). However, the relationships between the main group of clades were not completely concordant between the ML and BI analyses (Fig. 3).

The addition of indels slightly increased the branch lengths and the deeper node support in both ML and BI trees (Supplementary Data Fig. S3; Files S17 and S18). The

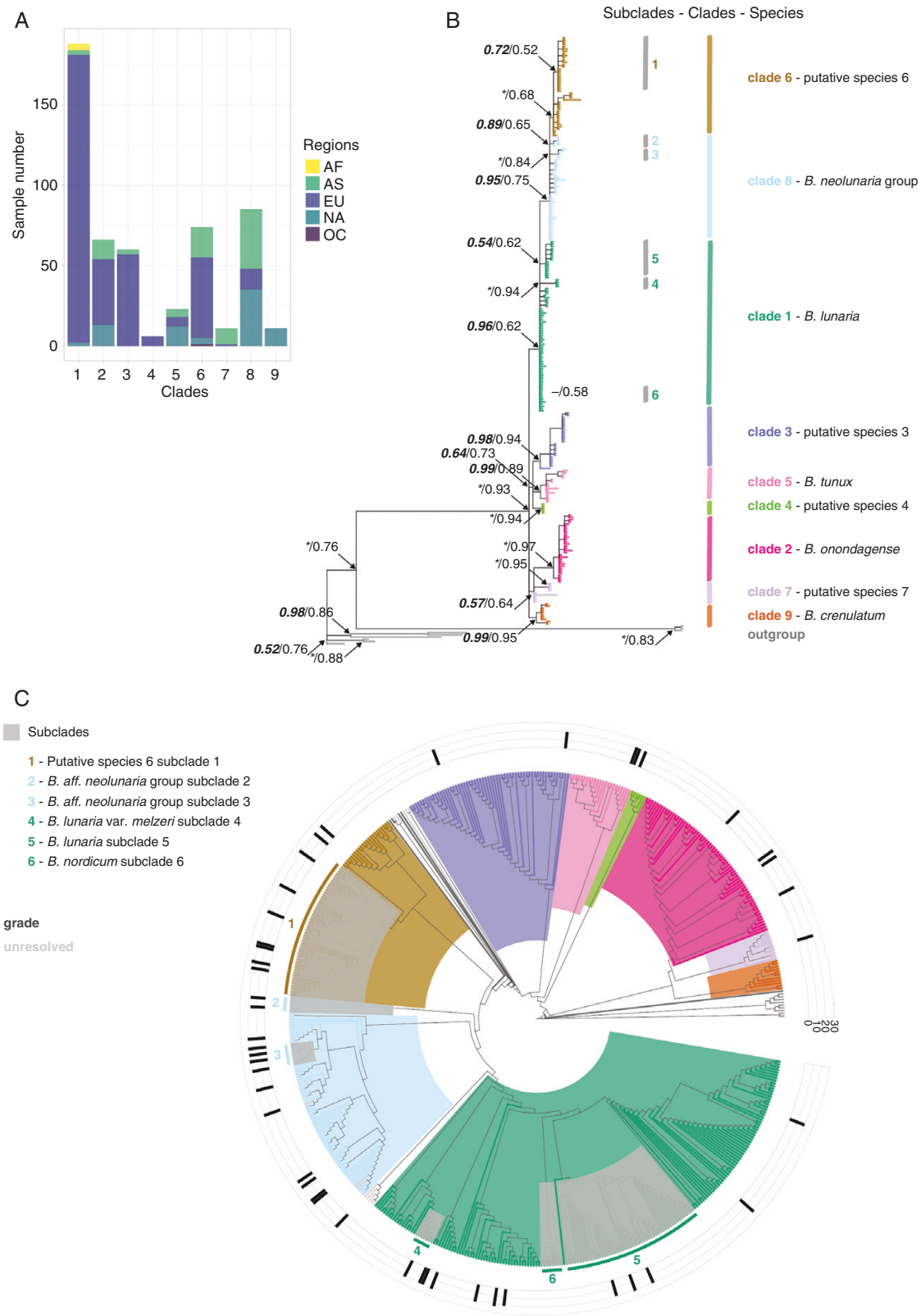

FIG. 2. Phylogenetic trees depicting the lineages of the *Botrychium lunaria* group with branch support values and genome size distribution. (A) Distribution of specimens grouped per clade by large geographical units. Abbreviations: AF, North Africa; AS, Asia; EU, Europe; NA, North America; OC, Oceania. (B) Phylogram of the BI tree (tree based on reduced dataset, A1). Bayesian inference posterior probabilities (BIPP) and ML bootstrap supports (MLBS) are on the left and right, respectively, along the main clade and subclade branches (i.e. *fully supported; -, not applicable; see Supplementary Data Files S17 and S18 for full BIPP and MLBS values, respectively). Each colour represents a distinct clade (tip labels are depicted in Supplementary Data Fig. S2). (C) Cladogram of the ML (tree based on complete dataset, A2 constrained with A1 indel tree backbone) tree in fan layout. Branch and background are coloured according to clades (tip labels are depicted in Supplementary Data Fig. S4). Grey layers on the top of the tree and coloured side bars indicate the subclade positions. The layer around the tree shows the absolute genome size distribution given in picograms for the 2C-values (for the values, see Supplementary Data Table S4).

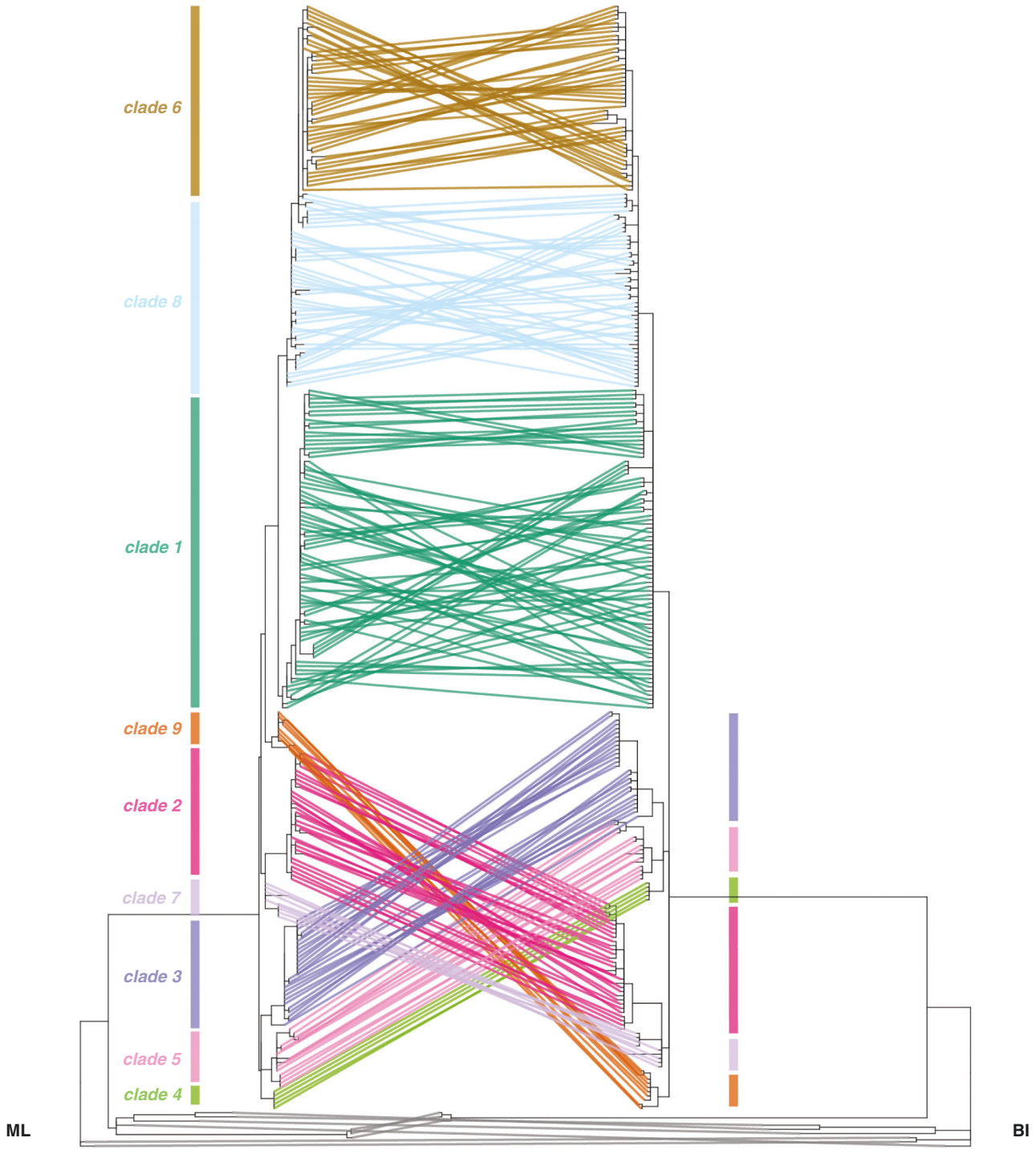

FIG. 3. Topological congruence of phylogenetic trees inferred from the reduced dataset (A1) using maximum likelihood (ML) and Bayesian inference (BI) methods. The tree on the right side corresponds to the BI tree and on the left side to the ML tree. Corresponding tips are linked by lines coloured according to clade assignment.

topologies recovered with indels were largely concordant with the analyses without, and individuals were assigned to the same clades, with few exceptions (Supplementary Data Fig. S3). The use of constrained topologies (Supplementary Data Files S19 and S20) for the ML analysis based on the full dataset (A2) allowed the assignment of most individuals with partial sequencing data and low phylogenetic signal. Nevertheless, the placement of a few specimens remained uncertain, probably owing to incomplete or unreliable sequence data. For example, the assignments of one rogue individual from the Alps (AM-lun33-3-CH) to a clade otherwise restricted to Eastern Asia (clade 7) or individuals from Central Asia (MW19 and

MW44-3) to a clade otherwise restricted to southeastern Europe (clade 6, subclade 1) were highly suspect (Supplementary Data Fig. S4). Moreover, specimens with wandering positions between the two A2 trees were marked as unresolved (Fig. 2C; Supplementary Data Fig. S4). The inference constraint by the backbone built with indels provided a better resolution of the deeper nodes than the backbone built without indels. Therefore, we retained this topology for further interpretations.

Some of the nine main clades recovered corresponded to previously recognized species (e.g. *B. tunux* and *B. crenulatum* corresponded to clades 5 and 9, respectively), whereas in other cases they combined recognized species, such as *B. neolunaria* and its polyploid derivate *B. yaaxudakeit* (clade 8; Fig. 2B). Interestingly, the single specimen sequenced from Turkey was consistently recovered as sister to the entire *B. lunaria* group. Some clades showed clear phylogenetic structure within them. We identified six such subclades (Fig. 2B, C). One was found in clade 6 (subclade 1), two were in clade 8 (subclades 2 and 3), and three were within clade 1, namely subclades 4 (*B. lunaria* var. *melzeri*), 5 and 6 (*B. nordicum*). Of these subclades, two correspond two described taxa, whereas the remaining four are geographically restricted (south-eastern Europe, mostly Balkans, central Alps, Baikal region and Carpathians; subclades 1, 5, 2 and 3, respectively). All except the *B. nordicum* subclade were recovered in the BI trees based on the reduced dataset. *B. nordicum* clade was supported solely in the ML tree based on the full dataset.

Assessments of ploidy level

The assessment of the ploidy level within the *B. lunaria* group indicated a dominant diploid condition. Absolute genome size showed no evidence of variation in ploidy level, with 2C-values of 55 specimens being between 19.38 and 22.91 pg, except for two individuals from clade 8, subclade 3 with 2C-values of 17.49 and 17.91 pg (Supplementary Data Table S4), which attest to a diploid condition (Veselý *et al.*, 2012; Williams and Waller, 2012; Dauphin *et al.*, 2016). Spore measurements made on 14 additional individuals showed a similar pattern, with one exception. Most had average lengths between 31 and 39 µm (Supplementary Data Table S5), which corresponds to the range found for the diploid *B. neolunaria* (Stensvold and Farrar, 2017). However, one specimen from the Caucasus Mountains had an average length of 43 µm, which enters the range estimated for the tetraploid *B. yaaxudakeit* (Stensvold *et al.*, 2002).

Species clade-level classification and candidate species

Well-supported monophyletic clades containing type material or independently identified specimens by allozyme markers (Stensvold, 2008; Stensvold and Farrar, 2017; D. Farrar, unpubl. data) of previously recognized species were assigned to the corresponding species, with clades 5, 1, 9 and 2 corresponding to *B. tunux*, *B. lunaria*, *B. crenulatum* and *B. onondagense*, respectively. Among these, *B. onondagense* was recently rehabilitated after being synonymized with *B. lunaria* (Gilman *et al.*, 2024). Our candidate species criterion of well-supported monophyly was not applicable to clade 8 because it contained both diploids and polyploids described as distinct species (i.e. *B. neolunaria* and *B. yaaxudakeit*; Stensvold *et al.*, 2002; Stensvold and Farrar, 2017). In this case, all the specimens of clade 8 were grouped under the name of *B. neolunaria* group, including tetraploids previously identified by allozymes (Stensvold 2002, 2008; D. Farrar, unpubl. data) as *B. yaaxudakeit*, specimens previously identified as *B. neolunaria* called *B. neolunaria s.s.*, and all remaining specimens known or assumed to be diploids. We did not treat all diploids as the species *B. neolunaria* because *B. neolunaria* is described as restricted to North America, and previously analysed specimens from Europe clustering with *B. neolunaria* were characterized as potential introgressed hybrids with *B. neolunaria* as the maternal parent (Stensvold, 2008; Stensvold and Farrar, 2017). The remaining four clades are proposed as putative new species and named by their clade numbers (putative species 3, 4, 6 and 7).

We also recognized five monophyletic clades nested within species, including the taxa *B. nordicum*, recognized at the species level, and *B. lunaria* var. *melzeri*, recognized at the variety level (Stensvold and Farrar, 2017). The remaining subclades nested within the *B. neolunaria* group (subclades 2 and 3), clade 1 (subclade 5) and clade 6 (subclade 1) are not treated at a taxonomical level, but their ecological distinctness was tested in the downstream analysis because they formed well-supported monophyletic groups with a restricted geographical distribution.

Divergence time estimates

Our age estimates suggest that the radiation of the *B. lunaria* group started at the end of the Miocene and extended to the Pliocene, ~45 Myr after the genus *Botrychium* diverged from its sister genera, *Japanobotrychium* and *Sceptridium* (Fig. 4A; Supplementary Data Fig. S5). The results are comparable between the two clock models, although the uncorrelated lognormal relaxed clock model recovered higher divergence time estimates for both genus- and species-level analyses (Fig. 4B; Supplementary Data Figs S5–S7; Folder S2). For example, the mean estimates of the crown ages of the genus *Botrychium* were 19.5 Myr (95 % highest posterior density 7.1–22.6 Myr) and 14.1 Myr (95 % highest posterior density 8.7–20.8 Myr) under the uncorrelated lognormal relaxed clock model and the strict clock model, respectively. The *B. lunaria* group arose in the Pliocene epoch (mean 3.7 Myr, 95 % highest posterior density 2.49–5.27 Myr), and the species within mostly diverged from one another during the Gelasian, the first Pleistocene age, at 2.58–1.8 Myr (Fig. 4C; Supplementary Data Figs S6 and S7). The subclades diverged from the remainder of the clade at the end of the Calabrian and Chibanian ages, the second and third quarter of the Pleistocene epoch at ~1 Myr (putative species 6, subclade 1) and ~0.2 Myr (*B. nordicum*), respectively (Fig. 4C; Supplementary Data Figs S6 and S7).

Distribution ranges of species in the *B. lunaria* group

Our classification into species results in the recognition of seven (*B. onondagense*, *B. tunux*, *B. lunaria* var. *melzeri*, *B. neolunaria*, *B. yaaxudakeit*, *B. crenulatum* and putative species 6) in North America (USA, Canada and Greenland), six

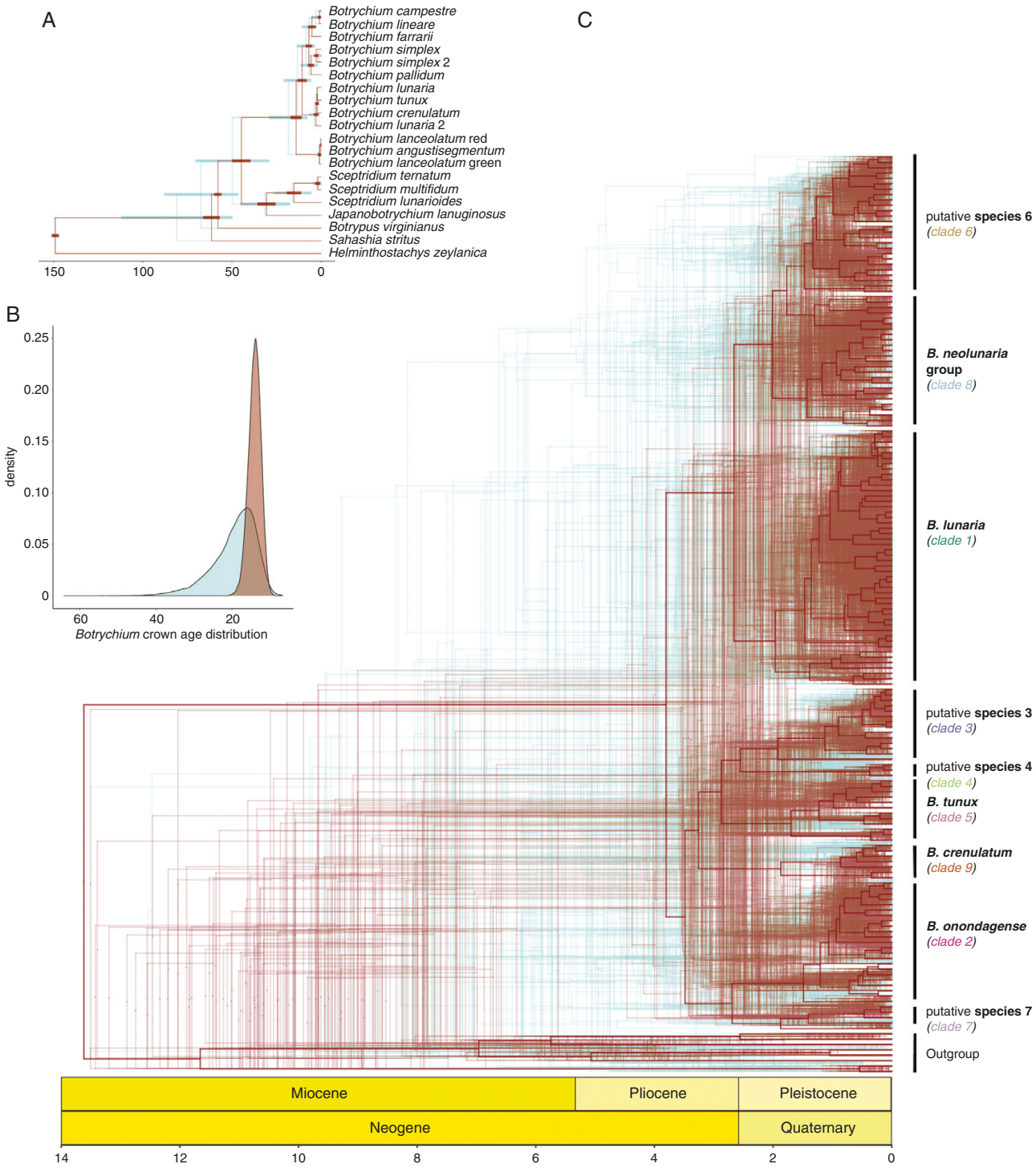

FIG. 4. Divergence time estimates of the subfamily Botrychioideae and of the species of the *Botrychium lunaria* complex. Time scales are in million-year units. The red colour refers to the divergence time analysis run under the strict clock model, and the blue colour to the relaxed clock model. (A) Time-calibrated phylogenies of the subfamily Botrychioideae. The 0.95 highest posterior density (HPD) is represented by bars at the calibrated nodes. (B) Distribution of the *Botrychium* crown age density estimated by the Botrychioideae time divergence analysis. (C) Time-calibrated phylogeny of the *B. lunaria* complex. The uncertainty around the node ages is displayed by density trees. The density trees were each drawn on a subset of 90 posterior trees. The geological time scale shows the periods and the epochs and follows the International Chronostratigraphic Chart (2018; https://stratigraphy.org).

(*B. lunaria*, *B. onondagense*, *B. tunux* and putative species 3, 6 and 7) in Asia, one each in northwestern Africa and Oceania (*B. lunaria* and putative species 6, respectively) and seven (*B. lunaria*, *B. nordicum*, *B. onondagense*, *B. tunux* and putative species 3, 4 and 6) to eight (considering the potential tetraploid from Georgia) species in Europe (Figs 2A and 5A–C). Of the

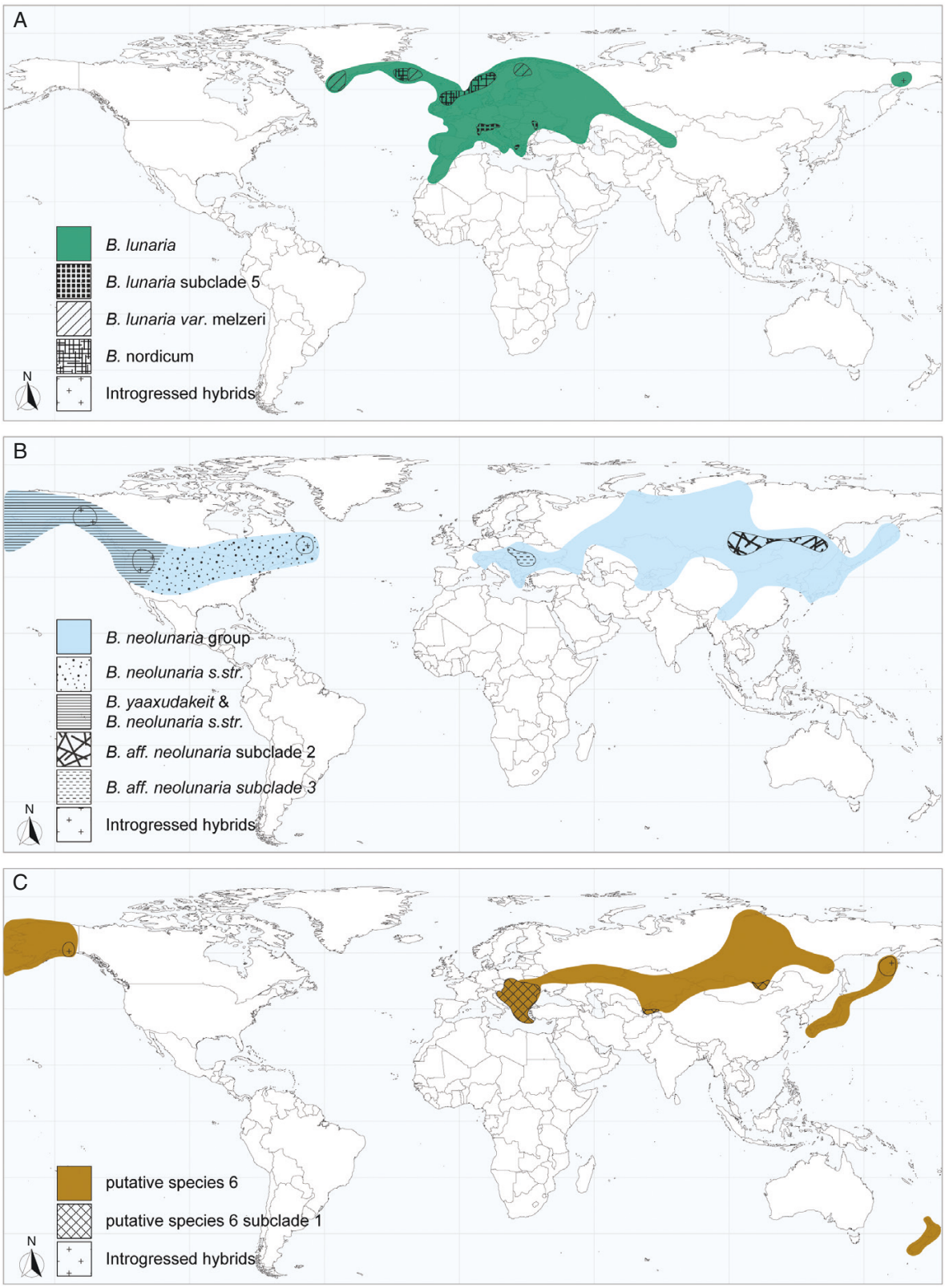

FIG. 5. Geographical distributions of the species of the *Botrychium lunaria* group. (A) Global distribution of *B. lunaria s.l.* (clade 1). (B) Global distribution of the *Botrychium neolunaria* group (clade 8). (C) Global distribution of the putative species 6 (clade 6).

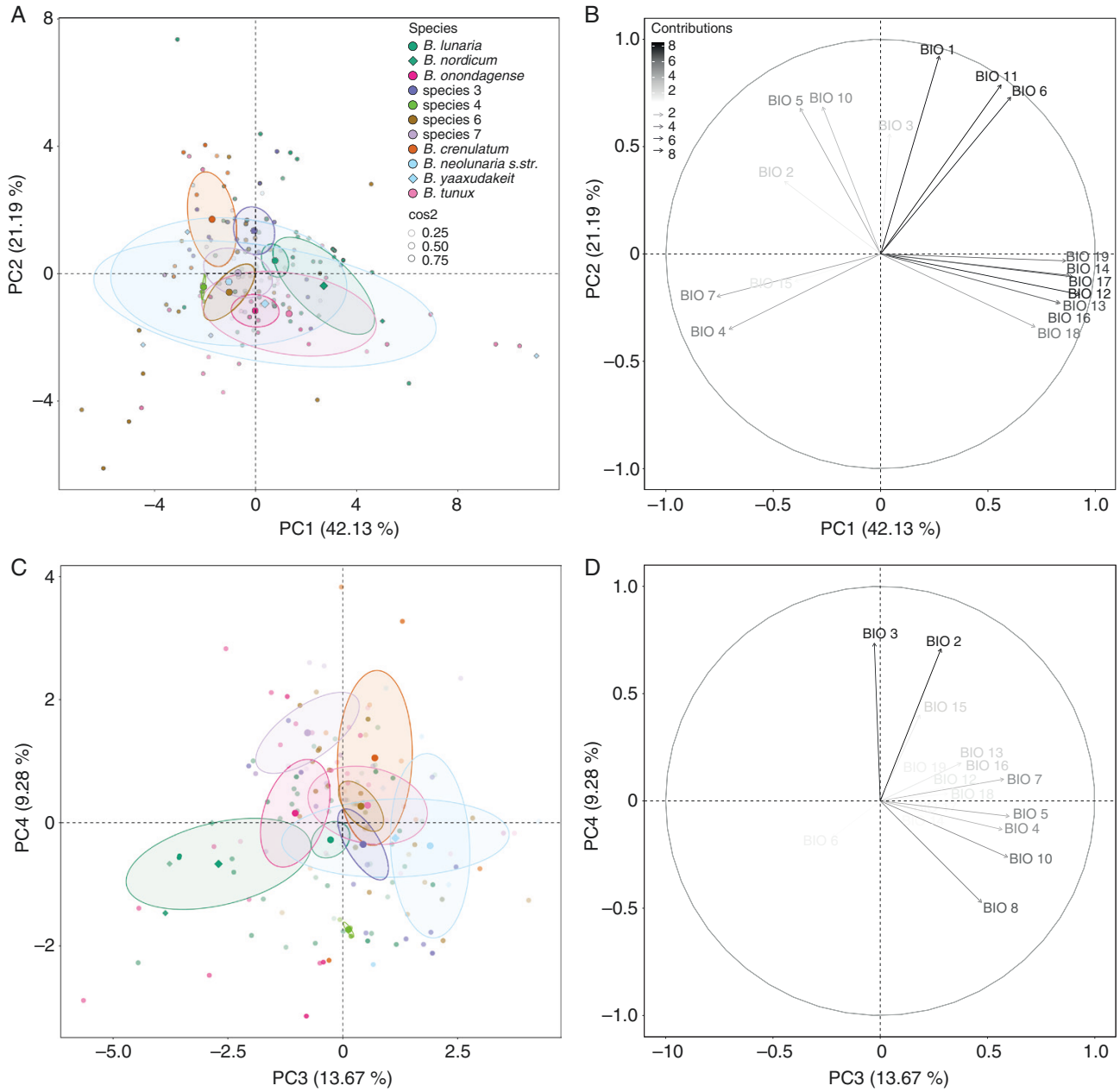

FIG. 6. Ecological differentiation between species of the *Botrychium lunaria* group. (A–D) Principal component analyses (PCAs) of climatic factors comparing the species occurrences. Point transparencies increase with lower cos2 values. Points and 95 % confidence ellipses are coloured according to clade assignment, with centroids indicated by larger circles. Arrow transparency represents the variable contributions to the principal component (PC). The definitions of the CHELSA bioclimatic variables are given in Supplementary Data Table S6. (A) Individual factor map, showing PC1 and PC2. (B) Variable factor map, showing PC1 and PC2. (C) Individual factor map showing the PC3 and PC4. (D) Variable factor map showing PC3 and PC4. (E) Boxplots of soil pH. The boxplot colours represent the pH mean per species. The grey dots show the distribution of the individual pH values, and their size is relative to the number of individuals with similar pH values. The sample size per species is given by *n*. (F) Maximum likelihood phylogenetic tree (based on complete dataset, A2 constrained with A1 indel tree backbone) depicted with collapsed clades. Triangle height relates to clade size and triangle width to the maximum branch length.

10 species level units found among our samples, four (putative species 4, 7, *B. crenulatum*, and *B. yaaxudakeit*) had narrow geographical ranges. These species were restricted to northern Europe, the Himalayas, as well as western and northern North America. The remaining species had wider distributions. For instance, *B. lunaria* (Fig. 5A) was recovered from northwestern Africa to Greenland and Central Asia. *Botrychium tunux* and *B. onondagense* both had a disjunct distribution in Europe and North America, with a disjunction between Eastern European and Central Asian populations, and no sample from western North America was assigned to *B. onondagense*. Putative species 3 and 6 were both found from Central and Eastern Europe to eastern Asia, with a marked disjunction in Central Asia for species 3 and a few records in Alaska for species 6. The most

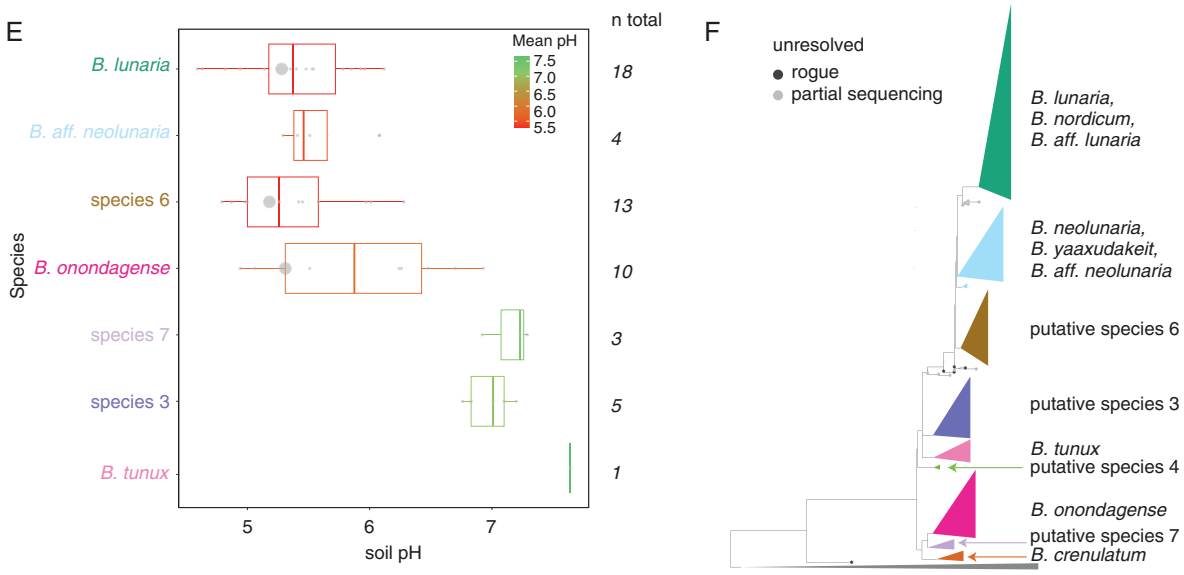

FIG. 6. Continued

widespread species-level group was the *B. neolunaria* group (Fig. 5B), which we recorded across almost the entire range of the *B. lunaria* group.

Climatic and soil analyses

The climatic niches largely overlapped between taxa, albeit with slight local differences. The PCA clustered the species into two groups. The first group consisted of *B. lunaria*, *B. crenulatum* and putative species 3, and the second group of *B. tunux*, *B. nordicum*, *B. onondagense*, *B. neolunaria s.s.*, *B. yaaxudakeit* and putative species 4, 6 and 7 (Fig. 6). The first component (PC1, 42.13 %) separated the species by temperature-related variables (BIO 1, 11 and 6), showing a gradient of strength of winter from mild winters (first group) to strong winters (second group) (Fig. 6A, B). The second component (PC2, 21.19 %) was correlated with precipitation-related variables (BIO 12, 13, 14, 16, 17, 18 and 19) and temperature seasonality (BIO 7 and 4), corresponding to a gradient of climatic continentality from less seasonal climates with high annual precipitations in areas close to oceans to strongly seasonal climates with low annual precipitations in continental regions. Within both groups, species were arranged along this continentality gradient. For example, in the second group, species were arranged from *B. nordicum* (oceanic) to species 4 (continental) (Supplementary Data Fig. S8). The third component (PC3, 13.67 %) was correlated with diurnal temperature fluctuations and their constancy through the year (BIO 2 and 3; Supplementary Data Fig. S8). Thus, the PCA 3 recovered that *B. crenulatum* and species 7 occur in habitats with a large range of diurnal and annual temperature fluctuations, with the former subjected to even stronger temperature variations.

We also observed differences in the climatic niches within clades with substructure (Supplementary Data Fig. S9). The PCA within clade 1 showed substantial climatic niche differentiation explained by seasonality (PC1, 45.32 %), high temperatures (PC2, 18.38%) and the strength of the winter (PC3, 16.11 %). In brief, *B. lunaria* var. *melzeri* occurred in dry climates with a strong seasonality and cold winters, *B. nordicum* in wet climates with low seasonality and low annual temperatures, and the two others in more temperate climates. The PCA within putative species 6 revealed similar importance of precipitation (PC1, 68.66 %) and seasonality (PC2, 13.25 %), with the nominal subspecies in dry habitats characterized by intermediate seasonality and cold winters and with subclade 1 in wet habitats characterized by low seasonality and mild winters. The PCA of the *B. neolunaria* group (clade 8) showed differences between *B. neolunaria s.s.* and the *B.* aff. *neolunaria* group related to summer temperature (PC1, 61.18 %) and seasonality (PC2, 28.33 %), with *B. neolunaria s.s.* and the *B.* aff. *neolunaria* group subclade 3 in climates with hot summers for the former, whereas the remainder of the *B.* aff. *neolunaria* group appeared to occur in climates with cold summers. Further, *B. neolunaria s.s.* occurs in climates with stronger seasonality than *B.* aff. *neolunaria*.

Soil pH showed differences between species, although the sample size was limited. *Botrychium lunaria*, *B.* aff. *neolunaria* group and putative species 6 were found only on acidic soils, whereas *B. tunux* and putative species 3 and 7 were recovered exclusively from neutral to basic soils (Fig. 6E, F; Supplementary Data Table S1). Interestingly, *B. onondagense* was found across the greatest range of pH values recorded in the *B. lunaria* group, with a trend towards the acidic soils.

DISCUSSION

Based on >500 sampled individuals, we provide the first global molecular phylogenetic analysis of the *B. lunaria* group. The lineage diversity recovered is congruent with previous, geographically more limited studies and uncovered two novel monophyletic clades, resulting in the recognition of 11 candidate taxa, including 7 previously described and 4 putative

novel species. These species-level units are evenly distributed throughout the Northern Hemisphere, with six to eight species per continent. We found little evidence that polyploidization played a role in the diversification of the group, although hybridization appears to be important in one clade. The time-calibrated phylogeny shows a concordance of Pleistocene climatic oscillations with the radiation of the group. Moreover, climate and soil pH showed slight differences at the species and subclade level, suggesting that ecological drivers played a role in the diversification of the *B. lunaria* group.

We freely acknowledge that one limitation of our study is that it includes only plastid regions, meaning that hybrids and polyploid individuals might not have been recognized in the absence of nuclear markers. However, as discussed below, the clades recovered by us make up consistent geographical and ecological units and support previous findings reported from allozyme markers (Stensvold *et al.*, 2002; Stensvold and Farrar, 2017), lending support to the notion that they are real evolutionary entities.

Taxonomic diversity in the *B. lunaria* group

Our plastid-based phylogeny recovered nine well-supported clades, of which two are novel (clades 6 and 7) compared with earlier studies based on the same plastid regions (Dauphin *et al.*, 2014, 2017; Maccagni *et al.*, 2017). The remaining seven clades are consistent with previous studies, although their relationships differ. Clades are arranged in three to four main groups in our analysis, against two in the previous studies. For example, clades 2 and 9 (*B. crenulatum*) were recovered as separated from each other in some of our analyses, whereas they were previously retrieved as sister clades (Dauphin *et al.*, 2017).

The nine clades found in the *B. lunaria* group include 12 candidate taxa. Seven of these correspond to currently accepted taxa, namely *B. lunaria* (Swartz, 1801), *B. crenulatum* (Wagner and Wagner, 1981), *B. tunux* (Stensvold *et al.*, 2002), *B. onondagense* (Underwood, 1903; Gilman *et al.*, 2024), *B. yaaxudakeit* (Stensvold *et al.*, 2002), *B. nordicum* (Stensvold and Farrar, 2017), *B. neolunaria* (Stensvold and Farrar, 2017) and *B. lunaria* var. *melzeri* (Stensvold and Farrar, 2017). Two other clades, namely putative species 3 and 4, have previously been recovered in phylogenetic analyses but have not been described (Dauphin *et al.*, 2014, 2017; Maccagni *et al.*, 2017). Finally, two clades are putative novel candidate taxa (species 6 and 7). This increased number of taxa is the result of our geographically more extensive sampling and overall increased sample size.

The consistency of the nine species-level clades in the ML and Bayesian analyses, despite different arrangements among the clades in the two analyses, in combination with their ecological and geographical distinctness, supports the notion that these clades are best treated at the species level. This is underpinned further by the fact that previously described species also recovered by us can be characterized morphologically (Wagner and Wagner, 1981; Stensvold *et al.*, 2002; Stensvold and Farrar, 2017). Although hybrids have been documented in the *B. lunaria* group (Stensvold, 2008), the fact that co-occurring species, such as *B. neolunaria* and *B. tunux* in North America (Fig. 1Ag), conserve their morphological and genetic distinctiveness suggests that these species are reproductively largely isolated (Wagner and Wagner, 1983*b*). Unfortunately, directly testing for reproductive isolation between lineages of the *B. lunaria* group by breeding experiments is restrained technically by the difficulty of cultivating the subterranean gametophytes (Campbell, 1911; Whittier, 1972, 1981; V. Mossion, unpubl. data). Nevertheless, we are confident that our treatment of the nine major clades recovered in our analyses as species is sound, along with the recognition of allotetraploid *B. yaaxudakeit* as a tenth species.

The taxonomic treatment of clades nested within the species-level clades is less straightforward, as exemplified by the case of *B. nordicum*, which was found to be nested deeply within *B. lunaria*, corroborating previous findings (Dauphin *et al.*, 2017). This taxon was described at the species level based on morphological distinctness and unique alleles separating it from *B.* '*lunaria*' (Stensvold and Farrar, 2017). In our analysis, this taxon was recovered as a monophyletic clade nested within *B. lunaria* such that treating it as specifically distinct would render the remainder of *B. lunaria* paraphyletic. Our divergence time estimates revealed that *B. nordicum* has only recently derived from the rest of *B. lunaria*, and its nested placement is thus likely to be the result of incomplete lineage sorting (Pamilo and Nei, 1988; Wendel and Doyle, 1998). We decided to refrain from formal taxonomic treatment of the subclades, pending further investigations involving nuclear sequencing data.

Finally, the *B. neolunaria* group presents special taxonomic problems. Not only does it include allotetraploid *B. yaaxudakeit*, which shares the plastid genome with its maternal parent, *B. neolunaria*, and thus cannot be distinguished with our data, but there also appears to be considerable genome size variation within this group. Our genome size measurements for Eurasian individuals of the *B. neolunaria* group showed much lower 2C-values (17.49–21.88 pg) than reported for 'true' *B. neolunaria* from North America (27.26–27.75 pg; Dauphin *et al.*, 2016). To date, no record of 'true' *B. neolunaria* identified by allozyme markers is known from Eurasia, although hundreds of plants have been analysed (Stensvold, 2008). However, specimens previously identified as fertile introgressed hybrids between *B. neolunaria* and *B.* '*lunaria*' have been recorded from Eurasia (Stensvold, 2008), thus while a considerable amount of our Eurasian samples cluster in the same clade as *B. neolunaria*, they might have different genetic backgrounds. Therefore, we propose that the differences in genome size in the *B. neolunaria* group reflect the presence of several taxa originating from multiple hybridization events between *B. neolunaria* and one or several other species from the *B. lunaria* group. We would not be surprised if this group contains several species-level taxa, but our plastid markers indicate only the maternal donor and do not allow us to test this hypothesis. Further studies involving nuclear markers are needed to address the evolutionary history and taxonomic diversity of the *B. neolunaria* group.

Global geographical distribution of the *B. lunaria* group

Based on intensive sampling in Western and Central Europe, Maccagni *et al.* (2017) proposed that continental Europe is the centre of diversity of the *B. lunaria* group. However, our geographically more exhaustive sampling shows that species numbers are evenly distributed between continents, with seven species in North America, seven to eight in Europe and six in

Asia. Importantly, our sampling is less dense in Asia (95 specimens, versus 357 specimens in Europe), with large areas yet to be sampled. It is thus conceivable that further species diversity might occur in Asia.

Dauphin *et al.* (2017) hypothesized that the *B. lunaria* group might have originated in Asia, because a clade composed mainly of Asian specimens was sister to the remainder of the group. Testing this hypothesis requires a firm resolution of the relationships between clades, which is not the case in our analysis. Indeed, the relationships between clades were inconsistent between the ML and BI methods. For example, the basal clade was not resolved in our BI trees, whereas the group of clades 4, 5 (*B. tunux*) and 3, which contain mostly European and North American specimens, was recovered as such in the ML trees (Fig. 3). It appears that our increased sampling size is not sufficient to resolve the deeper nodes and that additional sequencing data, preferably including nuclear data, are needed to address questions on the geographical origin of the *B. lunaria* group.

Considering the intensive previous studies in North America (Wagner and Wagner, 1981; Stensvold *et al.*, 2002; Stensvold, 2008; Stensvold and Farrar, 2017), it is unsurprising that most of the newly found candidate species have ranges restricted to Europe or Asia. Our study extends the known geographical distribution of most widespread species and confirms the narrow distribution of *B. crenulatum* (Wagner and Wagner, 1981; Stensvold, 2008; Dauphin *et al.*, 2017). Perhaps the most surprising range extension concerns the *B. neolunaria* group, which was previously known only from Eastern Asia, Oceania and North America (Dauphin *et al.*, 2017; Stensvold and Farrar, 2017) but was recorded by us across all Eurasia. However, disentangling the distribution of *B.* aff. *neolunaria* and 'true' *B. neolunaria* is not possible here because both share the same plastid genome. The same statement applies for the distribution of *B. yaaxudakeit*, the derivative polyploid of *B. neolunaria*.

Limited roles of polyploidization and hybridization in the diversification of the *B. lunaria* group

A previous study of other clades in the genus *Botrychium* has uncovered complex polyploid networks, revealing an important role of allopolyploidization in species formation in the genus (Dauphin *et al.*, 2018). In contrast, we found little evidence of ploidy variation within the *B. lunaria* group despite extensive sampling and additionally selecting morphologically aberrant specimens that might be hybrids. In combination with previous studies (Veselý *et al.*, 2012; Williams and Waller, 2012; Dauphin *et al.*, 2016), we thus show that the diploid condition is predominant in the *B. lunaria* group. This finding indicates that ploidy variation is not a major driver of diversification in the *B. lunaria* group, with the exception of allotetraploid *B. yaaxudakeit* (Stensvold *et al.*, 2002). Nevertheless, as detailed above, hybridization might have led to still poorly understood diversification in the *B. neolunaria* group.

Pleistocene climatic oscillations influenced the radiation of the *B. lunaria* group

Our study shows that the present species diversity of the *B. lunaria* group originated during the last 3 Myr, suggesting a possible link with the massive Pleistocene climatic fluctuations. Large parts of the current ranges of the species in the *B. lunaria* group were covered by ice during glacial times, including the entire known range of species 4 in boreal Scandinavia and most of the habitat of the species occurring in the Alps (Ivy-Ochs, 2015; Ehlers *et al.*, 2018). This is a well-known situation for alpine and boreal plant species that has frequently been invoked as driving the divergence of specific and intraspecific genetic differentiation by repeated cycles of extinction, migration, allopatry and sympatry (Tribsch and Schönswetter, 2003; Westergaard *et al.*, 2011). In the *B. lunaria* group, this has not resulted in the formation of primarily allopatric species as, for example, in the European gentians (Hungerer and Kadereit, 1998), but rather in the formation of numerous widespread species that mostly broadly overlap geographically and that often co-occur. For example, in the Swiss Alps, *B. tunux* has mostly been found in mixed populations with putative species 3, whereas *B. lunaria* subclade 5 and putative species 3 have also been recovered in sympatry (Maccagni *et al.*, 2017). In our study, we found similar patterns with, for example, *B. onondagense* and putative species 3 co-occurring at a site in Romania, or putative species 6 and *B. lunaria* co-occurring at several sites in Bosnia and Herzegovina. This co-occurrence of species is certainly a result of the high dispersal ability of ferns by their spores (Barrington, 1993), especially long-distance dispersal by wind, and attests to a highly dynamic history of population movements that cannot be reconstructed based on plastid data. Although hybrids are known to occur between species of the *B. lunaria* group (Stensvold, 2008), it is evident that species identity is not maintained primarily by limited gene flow between geographically remote populations, but rather by pre- or postzygotic mating barriers, which further supports the treatment of clades as species (Wagner *et al.*, 1985). However, whether original species divergence took place in sympatry or parapatry, or whether it was kick-started by allopatry, remains open to speculation.

Climatic and edaphic differentiation between species

We found that the climatic niches of the species within the *B. lunaria* group showed a certain degree of differentiation, but with marked overlap between many species. The main differentiation occurred along gradients of elevation (as reflected by various temperature-related variables) and climatic continentality. Unfortunately, the high uncertainty regarding species-level relationships within the main groups precludes conclusions about evolutionary tendencies related to species diversification within these clades. Overall, the climatic niche differentiation between species is relatively weak and unlikely to suggest that climatic divergence would be a major driver of diversification in the *B. lunaria* group.

Interestingly, however, in the analyses of climatic niches within variable species, we found that subclades were mostly better segregated in climatic niche space than the species. This is likely to reflect the fact that analyses within single species encompass a narrower range of climatic conditions in addition to fewer taxa, allowing for clearer segregation between taxa. Yet, considering that differentiation at the subclade level might be a precursor to species-level differentiation, and contrary to our conclusions above, this would suggest that climatic niche differentiation might indeed play an important role in the diversification of the *B. lunaria* group.

Our soil pH data from a subsample of sites also reveal patterns of edaphic preferences between species, with some species recorded only on neutral soils (*B. tunux* and putative species 3 and 7) and others on acidic soils (*B. lunaria*, *B.* aff. *neolunaria* group and putative species 6), although *B. onondagense* occurred across the entire pH range. Maccagni *et al.* (2017) also observed possible differences in habitat related to soil pH between two species (*B. lunaria* and our putative species 3). This suggests that there might be some degree of edaphic differentiation between species. In North America, *Botrychium* species have been found associated with calcareous bedrock, basalt bedrock and coastal soils influenced by ocean spray (D. Farrar, pers. obs.), with a higher species abundance and richness on neutral or basic soils (Farrar *et al.*, 2017).

Soil pH and temperature have been shown to explain the realized niche of arbuscular mycorrhizal fungi (AMF) (Davison *et al.*, 2021), with clear differences among *Glomus* species, which are known to be the main group of AMF associated with *Botrychium* species (Winther and Friedman, 2007; Sandoz *et al.*, 2020). Given that the growth of *Botrychium* is dependent on their AMF symbiosis, it might well be that pH preferences between species reflect association with distinct Glomeraceae species and that the co-evolution between AMF and *Botrychium* played a role in the diversification of the *B. lunaria* group.

In conclusion, we find that there is some ecological differentiation between species of the *B. lunaria* group, but evidence of this is rather weak, and at present we are unable to identify it as a prime driver of speciation in the group. Although limited, the soil data available to us evoke potential small-scale ecological differentiation that might not be recovered by our climatic data (at 1 km^2 resolution). We suggest that in-depth studies of ecological conditions and mycorrhizal fungi at sites where several species co-occur might help to improve our understanding of the role of ecological specialization in this group.

Conclusion

Based on a global sample of >500 specimens, our study reshapes the understanding of species-level diversity within the *B. lunaria* group and the geographical distribution of its diversity. We find that the timing of diversification corresponds to that of Pleistocene climatic oscillations, suggesting that diversification was driven mainly by repeated cycles of dispersal and extinction. This might then have been combined with some cases of polyploidization (*B. yaaxudakeit*, perhaps a further one in Georgia) and hybridization (in the *B. neolunaria* group), in addition to slight climatic and edaphic differentiation between many species. Although most of species-level taxa we recognize are 2–3 Myr old, the fact that we also found several much younger, genetically and climatically distinct subclades, suggests that diversification in the group is ongoing. Future studies should focus on clarifying the clade relationships within the *B. lunaria* group, on understanding the evolution and taxonomic implications of variation within the *B. neolunaria* group and on documenting the role of small-scale ecological differentiation between species.

SUPPLEMENTARY DATA

Supplementary data are available at *Annals of Botany* online and consist of the following.

Figure S1: boxplots of the differences between recognized and putative taxa for each bioclimatic variable. Figure S2: Bayesian inference (BI) tree based on reduced dataset (A1), with tip labels. Figure S3: effect of indels on the topology of trees inferred from the reduced dataset. Figure S4: maximum likelihood (ML) tree based on the full dataset (A2), with tip labels. Figure S5: time-calibrated phylogenies of the Botrychioidae subfamily genus. Figure S6: time-calibrated phylogeny of the *Botrychium lunaria* complex inferred under the strict clock model. Figure S7: time-calibrated phylogeny of the *Botrychium lunaria* complex inferred under the relaxed clock model. Figure S8: PCs 2 and 3 of the principal component analysis (PCA) at the species level. Figure S9: principal component analysis (PCA) at the subspecies level. Table S1: information about the specimens used in this study. Table S2: PCR protocols and thermocycling conditions developed in this study. Table S3: information about the sequences used in the divergence time analyses at the Botrychioideae subfamily level. Table S4: flow cytometry results. Table S5: spore length measurements. Table S6: CHELSA climatic variable meanings. File S1: multiple sequence alignment of the full dataset (A2) used for phylogenetic reconstruction. File S2: multiple sequence alignment of the reduced dataset (A1) including indels used for the phylogenetic reconstruction. File S3: multiple sequence alignment of the subfamily Botrychioideae used for the time divergence analyses. File S4: multiple sequence alignment A1 used for time divergence analyses. This alignment is an alignment containing no duplicated sequences produced by RAxML-NG. Folder S1, Files S5–S16: summaries of the ANOVA, principal component analysis eigenvalues and variable contributions. Files S17: Bayesian trees inferred from A1 alignment with and without scored indels including posterior probabilities. File S18: maximum likelihood tree inferred from A1 alignment with and without scored indels including bootstrap support values. File S19: maximum likelihood trees inferred from A2 alignment with bootstrap support values. File S20: RAxML-NG bestTrees of the phylogenetic trees inferred from A1 alignment (File S18) used to constrain the backbone of maximum likelihood trees inferred from A2 alignment (File S19). Folder S1: BEAST analysis files.

FUNDING

This work was supported by grants from the ‘Fond des donations’ and the ‘Subvention égalité’ of the University of Neuchâtel.

ACKNOWLEDGEMENTS

For their help organizing and carrying out fieldwork, we are in debt to Alexandru Coltoiu and the Bucegi Natural Park, Calimani National Park administration (Romania), Claudia Danau and the Retezat National Park (Romania), Clément Duckert, Cun-Feng Zhao, Daniel Ston, Kenan Ćatović, Kuban Uulu Zholdoshbek and the administration of Sarychat-Ertash State Nature Reserve (Kyrgyzstan), Luca Lässer, Marine Ramirez, Quentin Dubois, Sabin Neatu and the Ceahlau

National Park (Romania), Sandra Grünig, Sergei Aleksandrov and the Central Balkan National Park (Bulgaria), Shamil Shetekauri, Siqi Liang, Tolkha Shetekauri and the team of Tbilisi Botanical Garden (Georgia), Xianchun Zhang and Zikriyo. We are also thankful to Ahmed Ouhammou (MARK), Alessio Maccagni, Alexey P. Seregin (MW), Andreas Beiser, Dauphin Benjamin, Iowa State University (ISC), Filippo Prosser, Hedwig Meindl, Isabelle Chanaron (AIX), Markus Grabher, Natalia Gamova, Robin Walls, Sigitas Juzėnas, Siri Birkeland, Teddy Dolstra, Vincenzo Ferri, Wittmann Helmunt, Xian-Yun Mu and Xianchun Zhang (PE) for providing specimens. Many thanks to Amandine Pillonel, Ophélie Gning, Pierre-Emmanuel DuPasquier, Luyinda Lukau, Bondo Mateus and Benite Abayo who helped with the molecular laboratory work. Amandine Pillonel prepared the soil samples and made the *ex situ* pH measurements. Elke Kessler conducted the flow cytometry analyses. We thank Pierre-Emmanuel DuPasquier, Libing Zhang and Liang Zhang for the advanced access to Botrychioideae sequencing data. The computations were enabled by resources in project NAISS 2023/6-57 provided by the National Academic Infrastructure for Supercomputing in Sweden (NAISS) and Uppsala University at UPPMAX. Finally, we also acknowledge Sabina Moser Tralamazza and Ursula Oggenfuss for their thoughtful revisions of the manuscript.

AUTHOR CONTRIBUTIONS

V.M., J.G. and M.K. designed the study. J.G., M.K. and V.M. acquired the funding. V.M. organized and performed the fieldwork. D.R.F. provided essential type and identified reference plant material. E.K., V.M., D.C. and M.K. performed the analysis. M.K., V.M. and D.R.F. interpreted the results. V.M. and M.K. wrote the first draft, with substantial inputs from D.C. and D.R.F. All co-authors reviewed the manuscript and approved the final version.

Conflict of interest: None declared.

DATA AVAILABILITY

Sequences generated in this study were deposited on GenBank. The accession numbers are given in Supplementary Data Tables S1 and S3. Alignments and phylogenetic trees are available as Supplementary Data Files S1–S4 and S17–S20 (https://doi.org/10.5281/zenodo.13732351).

LITERATURE CITED

Abbott R, **Albach D**, **Ansell S**, ***et al***. **2013**. Hybridization and speciation. *Journal of Evolutionary Biology* **26**: 229–246.

Aberer AJ, **Krompass D**, **Stamatakis A. 2013**. Pruning rogue taxa improves phylogenetic accuracy: an efficient algorithm and webservice. *Systematic Biology* **62**: 162–166.

Allen GA, **Marr KL**, **McCormick LJ**, **Hebda RJ. 2012**. The impact of Pleistocene climate change on an ancient arctic–alpine plant: multiple lineages of disparate history in *Oxyria digyna*. *Ecology and Evolution* **2**: 649–665.

Alvarez N, **Thiel-Egenter C**, **Tribsch A**, ***et al***.; IntraBioDiv Consortium. **2009**. History or ecology? Substrate type as a major driver of partial genetic structure in Alpine plants. *Ecology Letters* **12**: 632–640.

Barrington DS. 1993. Ecological and historical factors in fern biogeography. *Journal of Biogeography* **20**: 275–279.

Bell MA, **Graeme TL. 2014**. strap: an R package for plotting phylogenies against stratigraphy and assessing their stratigraphic congruence. *Palaontology* **58**: 379–389. https://onlinelibrary.wiley.com/doi/10.1111/pala.12142.

Berry CM, **Hilton J. 2006**. Givetian (Middle Devonian) cladoxylopsid 'ferns' from Orkney, northern Scotland. *Transactions of the Royal Society of Edinburgh: Earth Sciences* **97**: 65–73.

Bozukov V, **Tsenov B**, **Vatsev M. 2010**. A first find of *Botrychium* (Ophioglossaceae) in Bulgarian palaeomacroflora. *Comptes Rendus de l'Académie bulgare des Sciences* **63**: 889–892.

Butters FK, **Abbe EC. 1953**. A floristic study of Cook county, Northeastern Minnesota. *Rhodora* **55**: 94.

Campbell DH. 1911. *The eusporangiate: the comparative morphology of the Ophioglossaceae and the Marattiaceae*. Washington, DC: Carnegie Institution of Washington.

Campitelli E. 2024. ggnewscale: multiple fill and colour scales in 'ggplot2'. *R package version 0.4.10*. https://CRAN.R-project.org/package=ggnewscale

Chang Y, **Li J**, **Lu S**, **Schneider H. 2013**. Species diversity and reticulate evolution in the *Asplenium normale* complex (Aspleniaceae) in China and adjacent areas. *TAXON* **62**: 673–687.

Charif D, **Lobry JR. 2007**. SeqinR 1.0-2: a contributed package to the R project for statistical computing devoted to biological sequences retrieval and analysis. In: **Bastolla U**, **Porto M**, **Roman HE**, **Vendruscolo M**, eds. *Structural approaches to sequence evolution. Biological and Medical Physics, Biomedical Engineering*. Berlin, Heidelberg: Springer, 207–232.

Clarke JM, **House HD. 1921**. Report of the state botanist for 1921. *New York State Museum Bulletin* **243-244**: 1–102.

Clausen RT. 1938. A monograph of the Ophioglossaceae. *Memoirs of the Torrey Botanical Club* **19**: 1–177.

Clute WN. 1905. A check list of the North American fernworts. *The Fern Bulletin* **13**: 109–123.

Cornish-Bowden A. 1985. Nomenclature for incompletely specified bases in nucleic-acid sequences. Recommendations 1984. *Nucleic Acids Research* **13**: 3021–3030.

Darriba D, **Posada D**, **Kozlov AM**, **Stamatakis A**, **Morel B**, **Flouri T. 2019**. ModelTest-NG: a new and scalable tool for the selection of DNA and protein evolutionary models. *Molecular Biology and Evolution* **37**: 291–294.

Dauphin B, **Vieu J**, **Grant JR. 2014**. Molecular phylogenetics supports widespread cryptic species in moonworts (*Botrychium* s.s., Ophioglossaceae). *American Journal of Botany* **101**: 128–140.

Dauphin B, **Grant J**, **Mráz P. 2016**. Ploidy level and genome size variation in the homosporous ferns *Botrychium* s.l. (Ophioglossaceae). *Plant Systematics and Evolution* **302**: 575–584.

Dauphin B, **Farrar DR**, **Maccagni A**, **Grant JR. 2017**. A worldwide molecular phylogeny provides new insight on cryptic diversity within the moonworts (*Botrychium* s. s., Ophioglossaceae). *Systematic Botany* **42**: 620–639.

Dauphin B, **Grant JR**, **Farrar DR**, **Rothfels CJ. 2018**. Rapid allopolyploid radiation of moonwort ferns (*Botrychium*; Ophioglossaceae) revealed by PacBio sequencing of homologous and homeologous nuclear regions. *Molecular Phylogenetics and Evolution* **120**: 342–353.

Davison J, **Moora M**, **Semchenko M**, ***et al***. **2021**. Temperature and pH define the realised niche space of arbuscular mycorrhizal fungi. *The New Phytologist* **231**: 763–776.

de Lafontaine G, **Napier JD**, **Petit RJ**, **Hu FS. 2018**. Invoking adaptation to decipher the genetic legacy of past climate change. *Ecology* **99**: 1530–1546.

De Queiroz K. 2007. Species concepts and species delimitation. *Systematic Biology* **56**: 879–886.

Des Marais DL, **Smith AR**, **Britton DM**, **Pryer KM. 2003**. Phylogenetic relationships and evolution of extant horsetails, *Equisetum*, based on chloroplast DNA sequence data (*rbcL* and *trnL-F*). *International Journal of Plant Sciences* **164**: 737–751.

Dolezel J, **Bartos J. 2005**. Plant DNA flow cytometry and estimation of nuclear genome size. *Annals of Botany* **95**: 99–110.

Doležel J, **Greilhuber J**, **Lucretti S**, ***et al***. **1998**. Plant genome size estimation by flow cytometry: inter-laboratory comparison. *Annals of Botany* **82**: 17–26.

Drummond AJ, **Suchard MA**, **Xie D**, **Rambaut A. 2012**. Bayesian phylogenetics with BEAUti and the BEAST 1.7. *Molecular Biology and Evolution* **29**: 1969–1973.

Dunnington D. 2025. ggspatial: spatial data framework for ggplot2. *R package version 1.1.9.9000*. https://github.com/paleolimbot/ggspatial

Ehlers J, **Gibbard PL**, **Hughes PD. 2011**. *Quaternary glaciations - extent and chronology. A closer look*. Amsterdam, The Netherlands: Elsevier, 2–1108.

Ehlers J, **Gibbard PL**, **Hughes PD. 2018**. Chapter 4 – Quaternary glaciations and chronology. In: **Menzies J**, **van der Meer JJM**, eds. *Past Glacial Environments*, 2nd edn. Amsterdam, The Netherlands: Elsevier, 77–101.

Farrar DR. 2011. *Systematics and taxonomy of genus Botrychium.* https://www.herbarium.iastate.edu/files/inline-files/Moonwort-Systematics.pdf (11 March 2016, date last accessed).

Farrar DR, **Johnson-Groh C. 1991**. A new prairie moonwort (*Botrychium* subgenus *Botrychium*) from northwestern Minnesota. *American Fern Journal* **81**: 1–6.

Farrar DR, **Gilman AV**, **Moran RC. 2017**. *Ophioglossales. Online edition. Naczi, R.F.C. New manual of vascular plants of northeastern United States and adjacent Canada*. NYBG Press, New York.

Frandsen PB, **Calcott B**, **Mayer C**, **Lanfear R. 2015**. Automatic selection of partitioning schemes for phylogenetic analyses using iterative *k*-means clustering of site rates. *BMC Evolutionary Biology* **15**: 13.

Garnier S, **Ross N**, **Rudis R**, ***et al***. **2024**. viridis(Lite) - Colorblind-Friendly Color Maps for R. viridis package version 0.6.5

Gastony GJ, **Yatskievych G. 1992**. Maternal inheritance of the chloroplast and mitochondrial genomes in Cheilanthoid ferns. *American Journal of Botany* **79**: 716–722.

Gearty W. 2024. deeptime: an R package that facilitates highly customizable visualizations of data over geological time intervals. *EarthArXiv*.

Gilman AV, **Farrar DR**, **Zika PF. 2015**. *Botrychium michiganense* sp. nov. (Ophioglossaceae), a new North American moonwort. *Journal of the Botanical Research Institute of Texas* **9**: 295–309.

Gilman AV, **Farrar DR**, **Stensvold MC. 2024**. *Botrychium onondagense* (Ophioglossaceae), a resurrected species in the North American *Botrychium lunaria* complex. *American Fern Journal* **114**: 57–65.

Guillon J-M, **Raquin C. 2000**. Maternal inheritance of chloroplasts in the horsetail *Equisetum variegatum* (Schleich.). *Current Genetics* **37**: 53–56.

Hanušová K, **Čertner M**, **Urfus T**, ***et al***. **2019**. Widespread co-occurrence of multiple ploidy levels in fragile ferns (*Cystopteris fragilis* complex; Cystopteridaceae) probably stems from similar ecology of cytotypes, their efficient dispersal and inter-ploidy hybridization. *Annals of Botany* **123**: 845–855.

Hauk WD. 1995. A molecular assessment of relationships among cryptic species of *Botrychium* subgenus *Botrychium* (Ophioglossaceae). *American Fern Journal* **85**: 375–394.

Hauk WD, **Parks CR**, **Chase MW. 2003**. Phylogenetic studies of Ophioglossaceae: evidence from *rbcL* and *trnL-F* plastid DNA sequences and morphology. *Molecular Phylogenetics and Evolution* **28**: 131–151.

Hauk WD, **Kennedy L**, **Hawke HM. 2012**. A phylogenetic investigation of *Botrychium* s. s. (Ophioglossaceae): evidence from three plastid DNA sequence datasets. *Systematic Botany* **37**: 320–330.

Hungerer KB, **Kadereit JW. 1998**. The phylogeny and biogeography of *Gentiana* L. sect. *Ciminalis* (Adans.) Dumort.: a historical interpretation of distribution ranges in the European high mountains. *Perspectives in Plant Ecology, Evolution and Systematics* **1**: 121–135.

Ivy-Ochs S. 2015. Glacier variations in the European Alps at the end of the last glaciation. *Cuadernos de Investigación Geográfica* **41**: 295–315.

Karger DN, **Conrad O**, **Böhner J**, ***et al***. **2017**. Climatologies at high resolution for the earth's land surface areas. *Scientific Data* **4**: 170122.

Karger DN, **Conrad O**, **Böhner J**, ***et al***. **2018**. Data from: Climatologies at high resolution for the earth's land surface areas [Dataset]. Dryad. https://doi.org/10.5061/dryad.kd1d4.

Kassambara A. 2023a. ggpubr: 'ggplot2' based publication ready plots. *R package version 0.6.0*. https://CRAN.R-project.org/package=ggpubr

Kassambara A. 2023b. rstatix: pipe-friendly framework for basic statistical tests. *R package version 0.7.2*. https://CRAN.R-project.org/package=rstatix

Kassambara A, **Mundt F. 2020**. factoextra: extract and visualize the results of multivariate data analyses.

Kato M. 1987. A phylogenetic classification of Ophioglossaceae. *The Gardens' Bulletin Singapore* **40**: 1–14.

Katoh K, **Standley DM. 2013**. MAFFT multiple sequence alignment software version 7: improvements in performance and usability. *Molecular Biology and Evolution* **30**: 772–780.

Khang T. 2016. Concatenation R. figshare. Software. https://doi.org/10.6084/m9.figshare.3839538.v1.

Kozlov AM, **Darriba D**, **Flouri T**, **Morel B**, **Stamatakis A. 2019**. RAxML-NG: a fast, scalable and user-friendly tool for maximum likelihood phylogenetic inference, *Bioinformatics* **35**: 4453–4455.

Kumar S, **Stecher G**, **Suleski M**, **Hedges SB. 2017**. TimeTree: a resource for timelines, timetrees, and divergence times. *Molecular Biology and Evolution* **34**: 1812–1819.

Kuo L-Y, **Tang T-Y**, **Li F-W**, ***et al***. **2018**. Organelle genome inheritance in *Deparia* ferns (Athyriaceae, Aspleniineae, Polypodiales). *Frontiers in Plant Science* **9**: 486.

Lê S, **Josse J**, **Husson F. 2008**. FactoMineR: an R package for multivariate analysis. *Journal of Statistical Software* **25**: 1–18.

Lehtonen S, **Silvestro D**, **Karger DN**, ***et al***. **2017**. Environmentally driven extinction and opportunistic origination explain fern diversification patterns. *Scientific Reports* **7**: 4831.

Lemoine F, **Entfellner J-BD**, **Wilkinson E**, ***et al***. **2018**. Renewing Felsenstein's phylogenetic bootstrap in the era of big data. *Nature* **556**: 452.

Lovis JD. 1958. An evolutionary study of the fern *Asplenium trichomanes. PhD thesis, University of Leeds*, p. 385.

Maccagni A, **Parisod C**, **Grant JR. 2017**. Phylogeography of the moonwort fern *Botrychium lunaria* (Ophioglossaceae) based on chloroplast DNA in the Central-European Mountain System. *Alpine Botany* **127**: 185–196.

Magallón S, **Hilu KW**, **Quandt D. 2013**. Land plant evolutionary timeline: gene effects are secondary to fossil constraints in relaxed clock estimation of age and substitution rates. *American Journal of Botany* **100**: 556–573.

Mickel JT, **Smith AR. 2004**. The pteridophytes of Mexico. *Memoirs of the New York Botanical Garden* **88**: 1–1054.

Milde J. 1869. Botrychium monographia. *Zoologisch-botanische gesellschaft in Wien. Verhandlungen* **19**: 55–190.

Muller S. 1986. *Botrychium matricariifolium* (Retz.) A. Braun ex Koch dans les pelouses sableuses du Pays de Bitche (Vosges du Nord). *Bulletin de la Société Botanique de France. Lettres Botaniques* **133**: 189–197.

Nekola JC, **Schlicht DW. 1996**. Distribution of *Botrychium campestre* in northeastern Iowa. *American Fern Journal* **86**: 119–123.

Neuwirth E. 2022. RColorBrewer: ColorBrewer palettes. *R package version 1.1-3*. https://CRAN.R-project.org/package=RColorBrewer

Pagel M, **Meade A**, **Barker D. 2004**. Bayesian estimation of ancestral character states on phylogenies. *Systematic Biology* **53**: 673–684.

Pamilo P, **Nei M. 1988**. Relationships between gene trees and species trees. *Molecular Biology and Evolution* **5**: 568–583.

Paradis E, **Schliep K. 2019**. ape 5.0: an environment for modern phylogenetics and evolutionary analyses in R. *Bioinformatics* **35**: 526–528.

Paris CA, **Wagner FS**, **Wagner WH Jr**. **1989**. Cryptic species, species delimitation, and taxonomic practice in the homosporous ferns. *American Fern Journal* **79**: 46–54.

Pebesma E. 2018. Simple features for R: standardized support for spatial vector data. *The R Journal* **10**: 439–446.

Popovich SJ, **Farrar DR**, **Gilman AV. 2020**. *Botrychium furculatum* (Ophioglossaceae), a new moonwort species from the Rocky Mountains of North America. *American Fern Journal* **110**: 165–182.

PPG I. **2016**. A community-derived classification for extant lycophytes and ferns. *Journal of Systematics and Evolution* **54**: 563–603.

Pryer KM, **Schuettpelz E**, **Wolf PG**, **Schneider H**, **Smith AR**, **Cranfill R. 2004**. Phylogeny and evolution of ferns (monilophytes) with a focus on the early leptosporangiate divergences. *American Journal of Botany* **91**: 1582–1598.

Qi X, **Kuo L-Y**, **Guo C**, ***et al***. **2018**. A well-resolved fern nuclear phylogeny reveals the evolution history of numerous transcription factor families. *Molecular Phylogenetics and Evolution* **127**: 961–977.

R Core Team. 2021. *R: a language and environment for statistical computing*. Vienna, Austria: R Foundation for Statistical Computing. https://www.R-project.org/

Rambaut A. 2009. *FigTree 1.4.4*. http://tree.bio.ed.ac.uk/software/figtree/ (17 January 2020, date last accessed).

Rambaut A, **Drummond AJ**, **Xie D**, **Baele G**, **Suchard MA. 2018**. Posterior summarization in Bayesian phylogenetics using Tracer 1.7. *Systematic Biology* **67**: 901–904.

Ravi V, **Khurana JP**, **Tyagi AK**, **Khurana P. 2008**. An update on chloroplast genomes. *Plant Systematics and Evolution* **271**: 101–122.

Revell LJ. 2012. phytools: an R package for phylogenetic comparative biology (and other things). *Methods in Ecology and Evolution* **3**: 217–223.

Rothfels CJ, **Larsson A**, **Kuo L-Y**, **Korall P**, **Chiou W-L**, **Pryer KM. 2012**. Overcoming deep roots, fast rates, and short internodes to resolve the

ancient rapid radiation of Eupolypod II ferns. *Systematic Biology* **61**: 490–509.
Rothfels CJ, **Johnson AK**, **Windham MD**, **Pryer KM. 2014**. Low-copy nuclear data confirm rampant allopolyploidy in the Cystopteridaceae (Polypodiales). *TAXON* **63**: 1026–1036.
Rothfels CJ, **Li F-W**, **Sigel EM**, ***et al***. **2015**. The evolutionary history of ferns inferred from 25 low-copy nuclear genes. *American Journal of Botany* **102**: 1089–1107.
Rothwell GW, **Stockey RA. 1989**. Fossil Ophioglossales in the Paleocene of Western North America. *American Journal of Botany* **76**: 637–644.
Salinas NR, **Little DP. 2014**. 2matrix: a utility for indel coding and phylogenetic matrix concatenation. *Applications in Plant Sciences* **2**: 1300083.
Sanderson MJ. 2002. Estimating absolute rates of molecular evolution and divergence times: a penalized likelihood approach. *Molecular Biology and Evolution* **19**: 101–109.
Sandoz FA, **Bindschedler S**, **Dauphin B**, **Farinelli L**, **Grant JR**, **Hervé V. 2020**. Biotic and abiotic factors shape arbuscular mycorrhizal fungal communities associated with the roots of the widespread fern *Botrychium lunaria* (Ophioglossaceae). *Environmental Microbiology Reports* **12**: 342–354.
Schneider C, **Rasband WS, Eliceiri K. 2012**. NIH Image to ImageJ: 25 years of image analysis. *Nature Methods* **9**: 671–675.
Schneider H, **Schuettpelz E**, **Pryer KM**, **Cranfill R**, **Magallón S**, **Lupia R. 2004**. Ferns diversified in the shadow of angiosperms. *Nature* **428**: 553–557.
Schönswetter P, **Stehlik I**, **Holderegger R**, **Tribsch A. 2005**. Molecular evidence for glacial refugia of mountain plants in the European Alps. *Molecular Ecology* **14**: 3547–3555.
Schuettpelz E, **Pryer KM. 2009**. Evidence for a Cenozoic radiation of ferns in an angiosperm-dominated canopy. *Proceedings of the National Academy of Sciences of the United States of America* **106**: 11200–11205.
Simmons MP, **Ochoterena H. 2000**. Gaps as characters in sequence-based phylogenetic analyses. *Systematic Biology* **49**: 369–381.
Small RL, **Lickey EB**, **Shaw J**, **Hauk WD. 2005**. Amplification of noncoding chloroplast DNA for phylogenetic studies in lycophytes and monilophytes with a comparative example of relative phylogenetic utility from Ophioglossaceae. *Molecular Phylogenetics and Evolution* **36**: 509–522.
Smith AR. 1972. Comparison of fern and flowering plant distributions with some evolutionary interpretations for ferns. *Biotropica* **4**: 4–9.
Smith MR. 2022. Using information theory to detect rogue taxa and improve consensus trees. *Systematic Biology* **71**: 1088–1094.
Solís-Lemus C, **Knowles LL**, **Ané C. 2015**. Bayesian species delimitation combining multiple genes and traits in a unified framework. *Evolution* **69**: 492–507.
South A. 2023. rnaturalearth: world map data from natural earth. *R package version 1.0.1*. https://CRAN.R-project.org/package=rnaturalearth
Ståhl P, **Ekman J**, **Westerberg S**, **Grant JR**, **Dauphin B. 2016**. Mer om pysslinglåsbräken i Sverige. *Svensk Botanisk Tidskrift* **110**: 2.
Stensvold MC. 2007. A taxonomic and phylogeographic study of the *Botrychium lunaria* complex. PhD thesis. Iowa State University. https://dr.lib.iastate.edu/handle/20.500.12876/69431
Stensvold MC, **Farrar DR. 2017**. Genetic diversity in the worldwide *Botrychium lunaria* (Ophioglossaceae) complex, with new species and new combinations. *Brittonia* **69**: 148–175.
Stensvold MC, **Farrar DR**, **Johnson-Groh C. 2002**. Two new species of moonworts (*Botrychium* subg. *Botrychium*) from Alaska. *American Fern Journal* **92**: 150–160.
Sukumaran J, **Holder MT. 2010**. DendroPy: a Python library for phylogenetic computing. *Bioinformatics* **26**: 1569–1571.
Sukumaran J, **Knowles LL. 2017**. Multispecies coalescent delimits structure, not species. *Proceedings of the National Academy of Sciences of the United States of America* **114**: 1607–1612.
Swartz O. 1801. Filicum, ordine systematico redactarum. *Journal für die Botanik* **1800**: 4–120.
Taylor TN, **Taylor EL**, **Krings M. 2009**. 11 – Ferns and early fernlike plants. In: **Taylor TN**, **Taylor EL**, **Krings M**, eds. *Paleobotany*, 2nd edn. London: Academic Press, 383–478.
Testo W, **Sundue M. 2016**. A 4000-species dataset provides new insight into the evolution of ferns. *Molecular Phylogenetics and Evolution* **105**: 200–211.
Tribsch A, **Schönswetter P. 2003**. Patterns of endemism and comparative phylogeography confirm palaeo-environmental evidence for Pleistocene refugia in the Eastern Alps. *Taxon* **52**: 477–497.
Underwood LM. 1903. An index to the described species of *Botrychium*. *Bulletin of the Torrey Botanical Club* **30**: 42–48.
Vasques DT, **Ebihara A**, **Hirai RY**, **Prado J**, **Motomi I. 2019**. Phylogeny of *Hymenophyllum* subg. *Mecodium* (Hymenophyllaceae), with special focus on the diversity of the *Hymenophyllum polyanthos* species complex. *Plant Systematics and Evolution* **305**: 811–825.
Veselý P, **Bureš P**, **Šmarda P**, **Pavlíček T. 2012**. Genome size and DNA base composition of geophytes: the mirror of phenology and ecology? *Annals of Botany* **109**: 65–75.
Vogel JC, **Russell SJ**, **Rumsey FJ**, **Barrett JA**, **Gibby M. 1998**. Evidence for maternal transmission of chloroplast DNA in the genus *Asplenium* (Aspleniaceae, Pteridophyta). *Botanica Acta* **111**: 247–249.
Wagner FS. 1993. Chromosomes of North American grapeferns and moonworts (Ophioglossaceae: *Botrychium*). *Contributions of the University of Michigan Herbarium* **19**: 83–92.
Wagner WH, **Grant JR. 2002**. *Botrychium alaskense*, a new moonwort from the interior of Alaska. *American Fern Journal* **92**: 164–170.
Wagner WH, **Lord LP. 1956**. The morphological and cytological distinctness of *Botrychium minganense* and *B. lunaria* in Michigan. *Bulletin of the Torrey Botanical Club* **83**: 261–280.
Wagner WH Jr, **Wagner FS. 1981**. New species of moonworts, *Botrychium* subg. *Botrychium* (Ophioglossaceae), from North America. *American Fern Journal* **71**: 20–30.
Wagner WH, **Wagner FS. 1982**. *Botrychium rugulosum* (Ophioglossaceae), a newly recognized species of evergreen grapefern in the Great Lakes area of North America [Pteridophyta; North Central States (USA)]. *Contributions from the University of Michigan Herbarium* **15**: 315.
Wagner WH, **Wagner FS. 1983***a*. Two moonworts of the Rocky Mountains; *Botrychium hesperium* and a new species formerly confused with It. *American Fern Journal* **73**: 53–62.
Wagner WH, **Wagner FS. 1983***b*. Genus communities as a systematic tool in the study of New World *Botrychium* (Ophioglossaceae). *TAXON* **32**: 51–63.
Wagner WH, **Wagner FS. 1986**. Three new species of moonworts (*Botrychium* subg. *Botrychium*) endemic in western North America. *American Fern Journal* **76**: 33–47.
Wagner WH, **Wagner FS. 1990***a*. Notes on the fan-leaflet group of moonworts in North America with descriptions of two new members. *American Fern Journal* **80**: 73–81.
Wagner WH, **Wagner FS. 1990***b*. Moonworts (*Botrychium* subg. *Botrychium*) of the upper Great Lakes region, U.S.A. and Canada, with descriptions of two new species. *Contributions from the University of Michigan Herbarium* **17**: 312–325.
Wagner WH, **Wagner FS. 1994**. Another widely disjunct, rare and local North American moonwort (Ophioglossaceae: *Botrychium* subg. *Botrychium*). *American Fern Journal* **84**: 5–10.
Wagner WH, **Wagner FS**, **Beitel JM. 1985**. Evidence for interspecific hybridisation in pteridophytes with subterranean mycoparasitic gametophytes. *Proceedings of the Royal Society of Edinburgh, Section B: Biological Sciences* **86**: 273–281.
Wang L-G, **Lam TT-Y**, **Xu S**, ***et al***. **2020**. Treeio: an R package for phylogenetic tree input and output with richly annotated and associated data. *Molecular Biology and Evolution* **37**: 599–603.
Wendel JF, **Doyle JJ. 1998**. Phylogenetic incongruence: window into genome history and molecular evolution. In: **Soltis DE**, **Soltis PS**, **Doyle JJ**, eds. *Molecular systematics of plants II: DNA sequencing*. Boston, MA: Springer US, 265–296.
Westergaard KB, **Alsos IG**, **Popp M**, **Engelskjøn T**, **Flatberg KI**, **Brochmann C. 2011**. Glacial survival may matter after all: nunatak signatures in the rare European populations of two west-arctic species. *Molecular Ecology* **20**: 376–393.
Whittier DP. 1972. Gametophytes of *Botrychium dissectum* as grown in sterile culture. *Botanical Gazette* **133**: 336–339.
Whittier P. 1981. Spore germination and young gametophyte development of *Botrychium* and *Ophioglossum* in axenic culture. *American Fern Journal* **71**: 13–19.
Wickham H. 2016. *ggplot2: elegant graphics for data analysis*. Springer International.
Wickham H, **Lin T** & **Seidel D. 2023**. scales: scale functions for visualization. *R package version 1.3.0*. https://CRAN.R-project.org/package=scales
Wickham H, **Averick M**, **Bryan J**, ***et al***. **2019**. Welcome to the Tidyverse. *Journal of Open Source Software* **4**: 1686.
Wikström N, **Kenrick P. 2001**. Evolution of Lycopodiaceae (Lycopsida): estimating divergence times from *rbcL* gene sequences by use of

nonparametric rate smoothing. *Molecular Phylogenetics and Evolution* **19**: 177–186.

Wilke CO. 2024. cowplot: streamlined plot theme and plot annotations for 'ggplot2'. *R package version 1.1.3*. https://CRAN.R-project.org/package=cowplot

Williams EW, **Waller DM. 2012**. Phylogenetic placement of species within the genus *Botrychium* s.s. (Ophioglossaceae) on the basis of plastid sequences, amplified fragment length polymorphisms, and flow cytometry. *International Journal of Plant Sciences* **173**: 516–531.

Williams EW, **Waller DM. 2015**. Tracking morphological change and demographic dynamics in ephemeral *Botrychium* s.s. (Ophioglossaceae) populations. *Journal of the Torrey Botanical Society* **142**: 152–165.

Williams EW, **Farrar DR**, **Henson D. 2016**. Cryptic speciation in allotetraploids: lessons from the *Botrychium matricariifolium* (Ophioglossaceae) complex. *American Journal of Botany* **103**: 740–753.

Winther JL, **Friedman WE. 2007**. Arbuscular mycorrhizal symbionts in *Botrychium* (Ophioglossaceae). *American Journal of Botany* **94**: 1248–1255.

Xu S. 2022. ggstar: Multiple Geometric Shape Point Layer for 'ggplot2'. *R package version 1.0.4*. https://CRAN.R-project.org/package=ggstar

Xu S, Dai Z, Guo P, **et al. 2021**. ggtreeExtra: Compact visualization of richly annotated phylogenetic data. *Molecular Biology and Evolution* **38**:4039–4042.

Yu G, **Smith DK**, **Zhu H**, **Guan Y**, **Lam TT-Y. 2017**. ggtree: an R package for visualization and annotation of phylogenetic trees with their covariates and other associated data. *Methods in Ecology and Evolution* **8**: 28–36.

Yu G, **Lam TT-Y**, **Zhu H**, **Guan Y. 2018**. Two methods for mapping and visualizing associated data on phylogeny using Ggtree. *Molecular Biology and Evolution* **35**: 3041–3043.

Zhang L, **Fan X-P**, **Petchsri S**, ***et al***. **2020**. Evolutionary relationships of the ancient fern lineage the adder's tongues (Ophioglossaceae) with description of *Sahashia* gen. nov. *Cladistics* **36**: 380–393.

Zhong B, **Fong R**, **Collins LJ**, **McLenachan PA**, **Penny D. 2014**. Two new fern chloroplasts and decelerated evolution linked to the long generation time in tree ferns. *Genome Biology and Evolution* **6**: 1166–1173.